

Passive Seismic Characterization of High Priority Salt Jugs in Hutchinson, Kansas: March 2023

Shelby L. Peterie, Julian Ivanov, Marcus Tamburro, Richard D. Miller, Brett C. Bennett,
Brett Wedel, Connor Umbrell, Cole Bunker, Carl Gonzales, and Olivia Jones

Kansas Geological Survey
1930 Constant Avenue
Lawrence, KS 66047



Draft Report to

Stephen R. Hoffine
Burns & McDonnell
9400 Ward Parkway
Kansas City, MO 64114
816-839-9526

The Kansas Geological Survey makes no warranty or representation, either express or implied, with regard to the data, documentation, or interpretations or decisions based on the use of this data including the quality, performance, merchantability, or fitness for a particular purpose. Under no circumstances shall the Kansas Geological Survey be liable for damages of any kind, including direct, indirect, special, incidental, punitive, or consequential damages in connection with or arising out of the existence, furnishing, failure to furnish, or use of or inability to use any of the database or documentation whether as a result of contract, negligence, strict liability, or otherwise. This study was conducted in complete compliance with ASTM Guide D7128-05. All data, interpretations, and opinions expressed or implied in this report and associated study are reasonably accurate and in accordance with generally accepted scientific standards.

Passive Seismic Characterization of High Priority Salt Jugs in Hutchinson, Kansas: March 2023

Executive Summary

This project appraised stress conditions of rock above selected dissolution voids by estimating the relative stress field from the calculated shear-wave velocity of the overburden. An estimate of change and potential hazard each void represents can be obtained by comparing the current stress conditions with those measured on the previous survey. Shear-wave velocities were calculated using passive surface-wave methods. Data were acquired along thirteen profiles located on or near key abandoned brine production wells with train traffic used as an energy source. The multichannel analysis of surface waves (MASW) method provided an estimate of the shear-wave velocity, at a resolution sufficient to loosely map the alluvial/bedrock contact and velocity characteristics of the Permian-aged shale above the top of the “three finger” dolomite (at approximately 100 meters below ground surface). A key outcome was the differentiation of relative rock stress based on shear velocity above salt jugs (associated with the target wells) compared to rocks above undisturbed salt or jugs without wide spans of unsupported roof rock. Comparisons of shear-wave velocity profiles over time (timelapse) provided insights into consistency of overburden stability and therefore indirectly, void dynamics.

Passive MASW data were continuously acquired over four nights (March 20-24, 2023) above wells with a potential to impact surface access or assets on the Vigindustries site in Hutchinson, Kansas. A continuous sampling approach targeting different wells each night was used to record all available train sources of passive source energy to maximize opportunities to capture energy with optimal source orientation and surface-wave characteristics. Surface waves were recorded with frequencies as low as approximately 4.5 hertz (Hz) representing an approximately 60 meter (m) average maximum depth of investigation, which generally represents a depth of more than 40 m below the bedrock surface.

Since shear modulus is the ratio of stress over strain and shear-wave velocity is a function of shear modulus and density, it is possible to estimate relative stress of overburden rocks (shear modulus) from shear-wave velocity values. Local increases in shear-wave velocity above background and without correlation to changes in lithology can be equated to increases in stress associated with changes in the distribution of overburden roof rock loading above dissolution jugs. Relative shear-wave velocity lows may be associated with remnants of a partial or incremental collapse whose vertical movement has been arrested by bulking or reduction in overburden stress due to redistribution within roof rock or changes in rock strength with vertical migration due to different geologic properties related to natural variation.

Overall shear-wave velocity directly over or in proximity to most of the 45 wells in this year’s study are consistent with natural geologic conditions and a normal stress regime as observed on previous years’ studies. Therefore, as in previous years, the 2023 results suggest that the shale overburden is currently in a state of relative stability with localized changes suggesting future vertical migration might be possible at less than a dozen wells. Overburden materials at seven wells from this March 2023 survey were interpreted to have subtle but notable changes in overburden characteristics relative to past years or expected for native conditions. Bedrock velocity at wells 2A and 4B, a major focus of past reports due to dynamic overburden conditions and possible limited failure at depth, has returned over the last year to an anisotropic velocity condition, suggesting dynamic changes continue in this area. Timelapse variability near 14B (line 5) may suggest dynamic stress changes associated with changes in roof structures or characteristics of the salt jug has occurred. Williams Street (line 9) is noted to have consistent velocity trends within the upper 30 m, but timelapse variability deeper than 30 m over the past few years and a notable decrease in velocity on the southern half of the line in 2023. These observations suggest the possibility of elevated stress on the northern part of the line spanning wells 52 and 53 and localized failure or redistribution of stress on the southern part of the line spanning wells 59 and 60.

Introduction

Material properties (specifically stress accumulations) measured as a function of depth above abandoned salt jugs in Hutchinson, Kansas, appear related to the mobility and upward migration of load density associated with the tensional dome of these jugs. Localized escalation in stress (as indicated by increased shear-wave velocity) above subterranean voids is one indicator of an increased potential for roof failure and void migration (Eberhart-Phillips et al., 1989; Dvorkin et al., 1996; Khaksar et al., 1999; Sayers, 2004). Previous studies, using both active and passive seismic wavefield characteristics, suggest perturbations in the shear-wave velocity field immediately above voids can be correlated to characteristics of the unsupported roof spans of salt jugs in the Hutchinson area (Sloan et al., 2010).

The strength of individual rock layers can be qualitatively described in terms of stiffness/rigidity and empirically estimated from relative comparisons of shear-wave velocity measurements. Shear-wave velocity is directly proportional to stress and inversely related to non-elastic strain. Since the shear-wave velocity of earth materials changes when stress and any associated elastic strain on those materials becomes “large,” it is reasonable to suggest load-bearing rock above mines or dissolution voids may experience elevated shear-wave velocities due to loading between pillars or, in the case of voids, loading between supporting side walls. This localized increase in shear velocity is not related to increased strength but to increased load as defined by Young’s Modulus. High-velocity shear-wave encompassing low-velocity anomalies (“halo” anomalies) are suggested to be key indicators of near-term roof failure. All these phenomena have been observed within the overburden above voids in the Hutchinson Salt Member in Hutchinson at depths greater than 30 m below the bedrock surface.

Previous research projects at the Carey Boulevard Research Area (CBRA) correlated measured shear-wave velocities with the condition of dissolution void roofs and the physical properties of the overburden at selected locations on Vigindustries legacy solution mining property in Hutchinson. In 2008, active seismic reflection was used to evaluate the effectiveness of shear-wave velocity to estimate local stress above voids representative in the size and depth as those prevalent at the Vigindustries site. It was determined that the integrity of the overlying strata could be reasonably estimated using shear-wave seismic reflection imaging. The lack of necessary ultra-low-frequency surface waves in the recorded wavefield have negated attempts to use active-source multi-channel analysis of surface waves (MASW) to estimate shear velocity in the lithified rocks above the voids and near the top of bedrock (Miller et al., 2009).

Uncontrolled local industrial and transportation activities represent sound sources that can produce the necessary low frequency seismic waves to interrogated rock material at depth greater than 60 m using passive methods (Miller, 2011). Key to this method is the ability to estimate shear-wave velocities using MASW to depths more than double those possible using standard active sources (Park et al., 2004). Results of passive MASW studies at and near this site suggest that this method is effective in identifying jugs with heightened risk for upward migration (Miller, 2011; Ivanov et al., 2013).

Following the active seismic imaging study in 2008, two-dimensional (2-D) passive MASW surveys were acquired at the CBRA between 2012 and the present to appraise the stability of overburden at selected wells (Table 1). Results of these investigations suggested a normal stress regime with natural geologic variation in most wells. Shear velocity above a few wells was noted to be outside what might be considered normal for the area and justified more attention. Individually, each profile represents a snapshot in time. When combined with previous observations at the same locations, timelapse analysis can be used to monitor for temporal variation in shear velocity, providing insight into relative stability and void dynamics.

Table 1. Dates of wells evaluated during 2-D passive MASW surveys at the CBRA.

Date	Wells
August 2012	2A, 1B, 2B, 3B, 5B, 6B, 7B, 12B
October 2012	2B, 4B, 6B, 17, 45, 52, 53, 59
March 2013	2A, 4B
November 2014	2A, 3B, 4B
March 2015	1B, 2B, 3B, 6B, 8A, 8B, 10B, 11B, 12B, 13B, 14B, 15B, 17, 18, 22A, 23, 23B, 29, 30, 39, 41, 42, 44, 45, 46, 86, 87, 88, 89, 90, 92
May 2015	2A, 4B
June 2015	4A, 6B, 7A, 7B, 52, 53, 59, 60
November 2017	2A, 4A, 7A, 8A, 1B, 2B, 3B, 4B, 6B, 7B, 8B, 10B, 11B, 12B, 13B, 14B, 15B, 17, 18, 22A, 23, 23B, 29, 30, 39, 41, 42, 44, 45, 46, 52, 53, 59, 60, 86, 87, 88, 89, 90, 92
October 2018	2A, 4B
December 2018	1B, 2B, 3B, 4A, 4B, 6B, 7A, 7B, 8A, 8B, 10B, 11B, 12B, 13B, 14B, 15B, 17, 18, 22A, 23B, 23, 29, 30, 39, 41, 42, 44, 45, 46, 52, 53, 59, 60, 86, 87, 88, 89, 90
December 2019	1B, 2A, 2B, 3B, 4A, 4B, 5B, 6B, 7A, 7B, 8A, 8B, 10B, 11B, 12B, 13B, 14B, 15B, 17, 18, 22A, 23B, 23, 29, 30, 39, 42, 44, 45, 46, 52, 53, 59, 60, 88, 89, 90, 92
August 2020	2A, 4A, 7A, 15B, 59
November 2020	1B, 2A, 2B, 3B, 4A, 4B, 5B, 6B, 7A, 7B, 8A, 8B, 10B, 11B, 12B, 13B, 14B, 15B, 17, 18, 22A, 23B, 23, 29, 30, 39, 42, 44, 45, 46, 52, 53, 59, 60, 88, 89, 90, 92
November 2021	1B, 2A, 2B, 3B, 4A, 4B, 5B, 6B, 7A, 7B, 8A, 8B, 10B, 11B, 12B, 13B, 14B, 15B, 17, 18, 19, 20, 22A, 23B, 23, 25, 26, 29, 30, 33, 36, 39, 41, 42, 44, 45, 46, 52, 53, 59, 60, 88, 89, 90, 92, 94
March 2023	1B, 2A, 2B, 3B, 4A, 4B, 5B, 6B, 7A, 7B, 8A, 8B, 10B, 11B, 12B, 13B, 14B, 15B, 17, 18, 19, 20, 22A, 23B, 23, 25, 26, 29, 30, 33, 36, 39, 41, 42, 44, 45, 46, 52, 53, 59, 60, 88, 89, 90, 92, 94

Geologic and Geophysical Setting

The Permian-aged Hutchinson Salt Member occurs in central Kansas, northwestern Oklahoma, and the northeastern portion of the Texas panhandle and is prone to and has an extensive history of dissolution and formation of sinkholes (Figure 1). In Kansas, the Hutchinson Salt Member possesses an average net thickness of 75 m and reaches a maximum of more than 150 m in the southern part of the basin. Deposition occurring during fluctuating sea levels caused numerous halite beds, 0.2 to 3 m thick, to be formed interbedded with shale, minor anhydrite, and dolomite/ magnesite. Individual salt beds may be continuous for only a few miles despite the remarkable lateral continuity of the salt as a whole (Walters, 1978).

The distribution and stratigraphy of the salt is well documented (Dellwig, 1963; Holdoway, 1978; Kulstad, 1959; Merriam, 1963). The salt reaches a maximum thickness in central Oklahoma and thins to depositional edges on the north and west, erosional subcrop on the east, and facies changes on the south. The increasing thickness toward the center of the salt bed is due to a combination of increased salt and more and thicker interbedded anhydrites. The Stone Corral Formation (a well-documented seismic marker bed) overlies the salt throughout

Kansas (McGuire and Miller, 1989). Directly above the salt at this site is a thick sequence of Permian shale.

The upper 760 m of rock at this site is Permian shale (Merriam, 1963). The Chase Group (top at 300 m deep), lower Wellington Shale (top at 245 m deep), Hutchinson Salt (top at 120 m deep), upper Wellington Shale (top at 75 m deep), and Ninnescah Shale (top at 25 m deep) make up the packets of reflecting events easily identifiable and segregated within the Permian portion of the section (Figure 2). Bedrock is defined as the top of the Ninnescah Shale with the unconsolidated Pliocene-Pleistocene Equus beds making up the majority of the upper 30 m of sediment. The thickness of Quaternary alluvium that fills the stream valleys and paleosubsideance features goes from 0 to as much as 90 m, depending on the dimensions of the features.

Recent dissolution of the salt and resulting subsidence of overlying sediments forming sinkholes has generally been associated with mining or saltwater disposal (Walters, 1978). Historically, these sinkholes can manifest themselves as a risk to surface infrastructure. The rate of surface subsidence can range from gradual to very rapid. Besides risks to surface structures, subsidence features potentially jeopardize the natural segregation of groundwater aquifers, greatly increasing their potential to negatively impact the environment (Whittemore, 1989, 1990). Natural sinkholes resulting from dissolution of the salt by localized leaching within natural flow systems that have been altered by structural features (such as faults and fractures) are not uncommon west of the main dissolution edge (Merriam and Mann, 1957).

Caprock and its characteristics are a very important component of any discussion concerning dissolution, subsidence, and formation of sinkholes. The Permian shales (Wellington and Ninnescah) that overlie the Hutchinson Salt Member are about 60 m thick in this area and are characterized as generally unstable when exposed to freshwater, being susceptible to sloughing and collapse (Swineford, 1955). These Permian shales tend to be red or reddish-brown and are commonly referred to as “red beds.” Permian red beds are extremely impermeable to water and have provided an excellent seal between the freshwaters of the Equus beds and the extremely water-soluble Hutchinson Salt Member. The modern-day expanse and mere presence of the Hutchinson Salt is due to the protection from freshwater provided by these red beds.

Isolating the basal contact of the Wellington Formation provides key insights into the general strength of roof rock expected, if dissolution-mined salt jugs (salt jugs are the jug-shaped

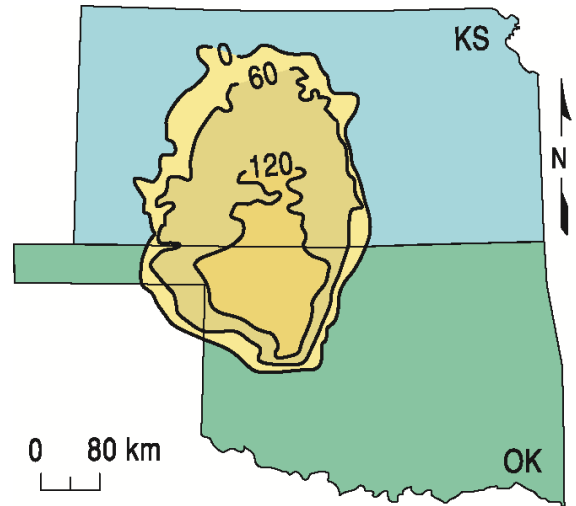


Figure 1. Approximate extent of salt formation, with contour intervals expressed in meters.

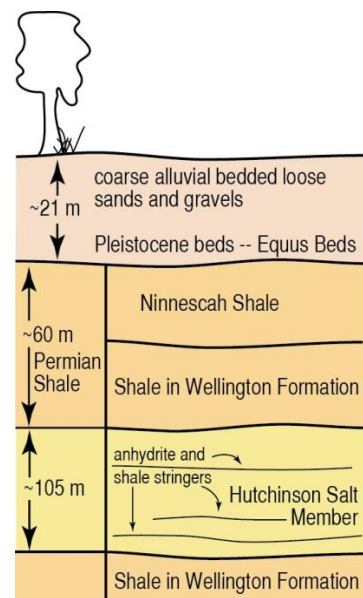


Figure 2. Generalized geology.

cavities or voids in the salt that form after salt has been dissolution mined in proximity to the wells) reach the top of the salt zone. Directly above the salt/shale contact is approximately 6 m thick dark-colored shale with joint and bedding cracks filled with red halite (Walters, 1978). Once unsaturated brine comes in contact with this shale layer, these red halite-filled joints and bedding planes are rapidly leached, leaving an extremely structurally weak layer.

Field Layout and Data Acquisition

To ensure the highest quality (e.g., signal-to-noise ratio, S/N) data and maximum crew safety, receivers were deployed during daylight hours and train data were recorded at night when cultural and industrial noise was minimal, thereby providing the highest possible S/N. Analysis of previous seismic energy sources captured during passive recording at this site clearly indicated trains at distances of 2 kilometers (km) or more provided the best broad spectrum, low-frequency seismic energy (Miller, 2011). Since seismic energy with characteristics best suited for this study may arrive when trains are at distances greater than can be detected by spotters, seismic energy was recorded continuously throughout the night to capture of all times, ensuring optimum data.

Data were acquired March 20-23, 2023. A total of thirteen seismic lines (Figure 3) were deployed during the day over this four-day period. Line layout was designed to cross directly over all wells of interest. A 2-D square grid of receivers was recorded simultaneously to allow determination of the incident orientation of passive seismic energy. Seismic receivers were single ION 4.5 Hz geophones spaced at 3 m intervals. The seismic lines collectively totaled approximately 5000 m in length. The 2-D monitoring/alignment grid consisted of 128 receivers spaced at 5 m intervals and was configured to form four concentric expanding squares with 10, 30, 50, and 70 m sides (Figure 4). Data were recorded with a 400+ channel 24-bit Geometrics Geode distributed seismic system. Line 15 and the 2-D grid utilized a wireless nodal acquisition system by GTI that recorded output from the geophones. Seismic records from the Geometrics system were 30 seconds (s) long with a 2 millisecond (ms) sampling interval. In total, 3558 seismic records were recorded.

Processing and Analysis

Data were processed using algorithms developed at the Kansas Geological Survey (KGS). The passive method used for this study is well published and has consistently proven effective producing good-quality results on other studies (Park et al., 2004; Ivanov et al., 2013). The continuous-data-acquisition method records energy from nearby sources at various orientations with respect to the seismic line. Data from the 2-D grid are evaluated for optimized source alignment with respect to each 1-D seismic line allowing data rotation and analysis or direct analysis of only data from near in-line sources.

For each line, the surface-wave amplitudes recorded by the 2-D grid were plotted as phase velocity versus frequency across a range of azimuths (0 to 360 degrees) (Figure 5), relative to the seismic line. This display was effective for identifying the best broad-band, low-frequency source energy with an azimuth as near zero as possible. Seismograms for each line were selected and segmented into the shortest groups of receivers (“spread length”) with optimum source characteristics that resulted in dispersion patterns on phase velocity versus frequency plots with the

greatest percentage of high-amplitude fundamental-mode Rayleigh-wave energy and minimal higher-order surface-wave interference (Figure 6).



Figure 3. Aerial photo with GPS locations of thirteen seismic lines, 2-D grid of receivers (orange squares), and wells in the November 2021 study.

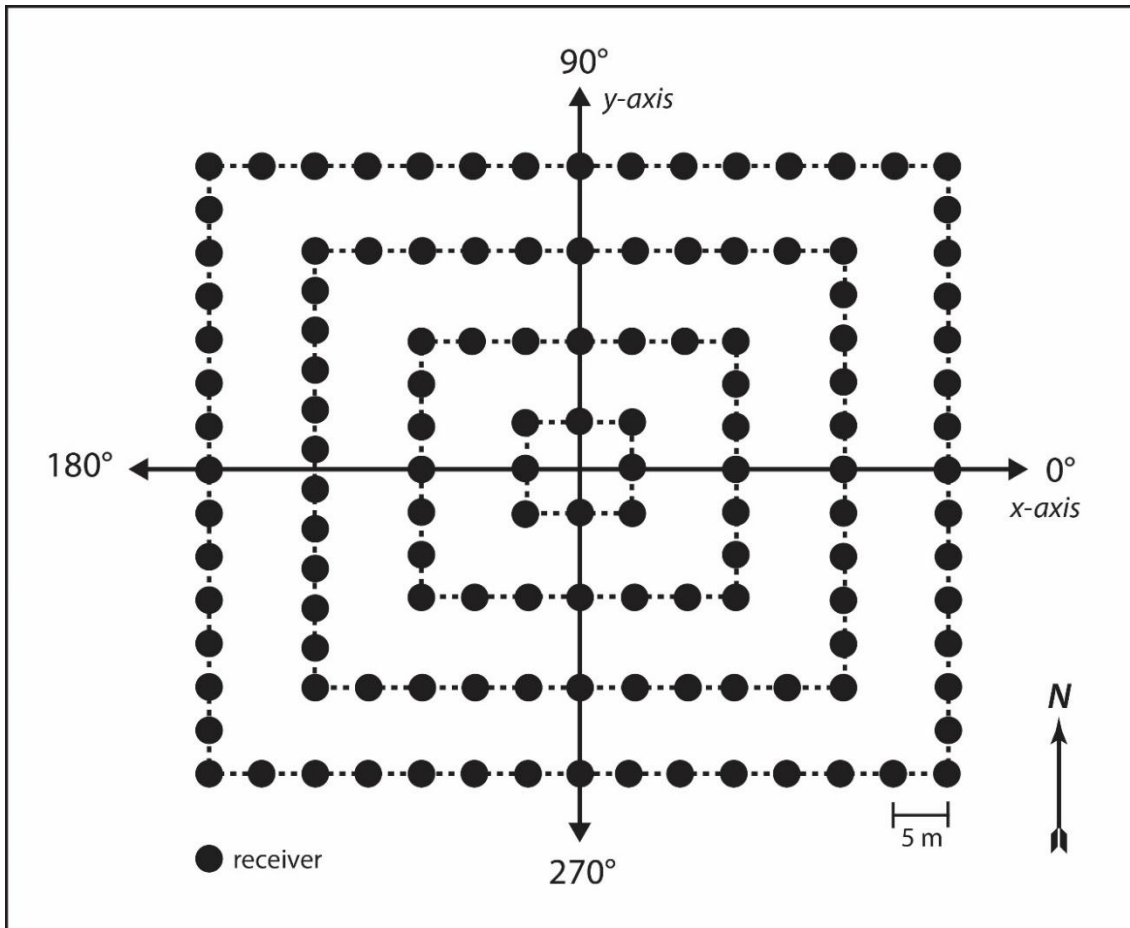


Figure 4. Four nested square arrays were deployed each night to construct the 2-D square grid for determining incident source azimuth information.

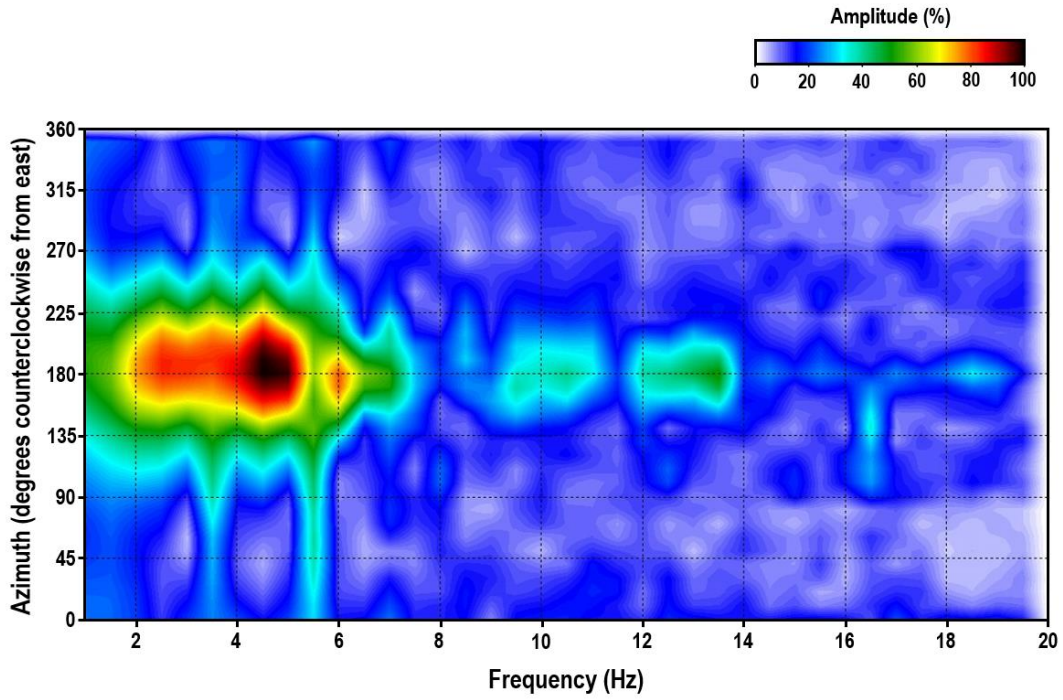


Figure 5. Azimuth plot indicating the direction of the dominant passive source energy (in degrees counterclockwise from east). Here, the dominant passive source energy is centered on approximately 180°.

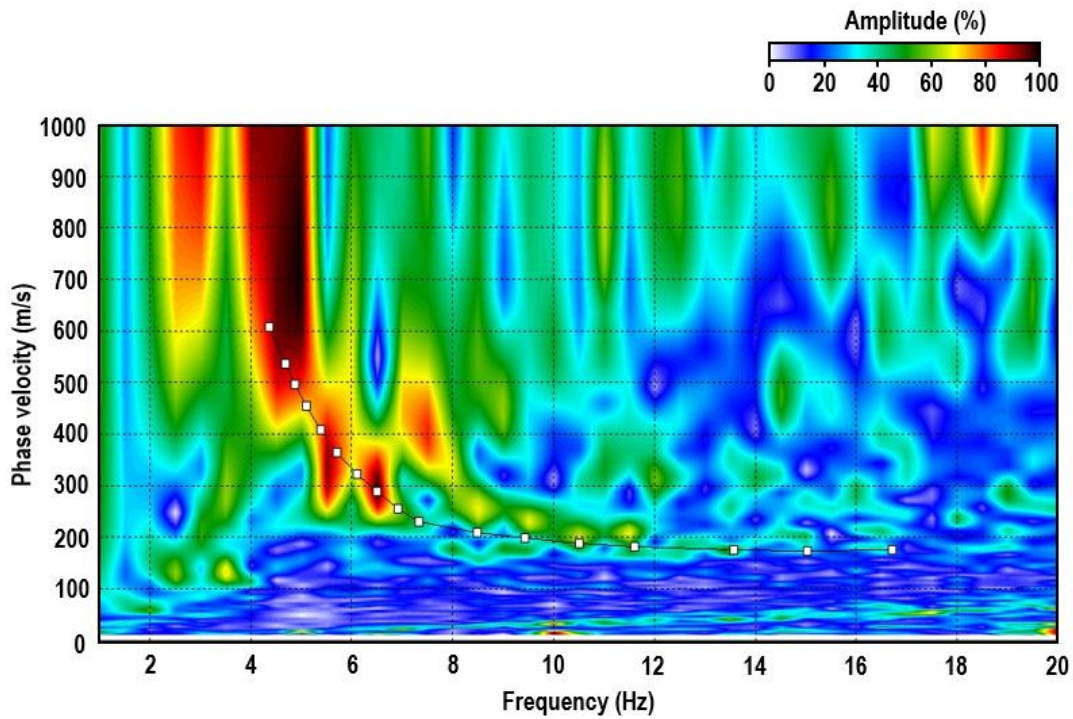


Figure 6. Dispersion pattern with high signal-to-noise ratio of the fundamental-mode Rayleigh wave.

Fundamental mode dispersion curves were picked and inverted to obtain a 2-D section of shear-wave velocity as a function of depth. The apparent velocity (v_{app}) is:

$$v_{app} = \frac{v_{act}}{(\cos \theta)} \quad (1)$$

where v_{act} is the actual seismic velocity and θ is the azimuth of the source with respect to the seismic line determined from the azimuth versus frequency plot. Thus, the percent increase in velocity (Δv) is:

$$\Delta v = \frac{1}{\cos \theta} - 1 \quad (2)$$

Equation 2 was used to calculate the increase in velocity due to the source azimuth for each line (Table 2).

Table 2. Directions of the passive seismic sources and the seismic lines; spread length used for processing, the angle of the source with respect to the line (θ , in degrees counterclockwise from east), and the percent increase in apparent velocity (Δv) attributable to oblique source orientations.

	processing spread length(s)	source orientation	line orientation	θ	Δv
Line 1	90 m	150°	135°	15°	3.53%
	99 m	0°	180°	180°	0%
Line 3	99 m	180°	180°	0°	0%
Line 4	81 m	180°	180°	0°	0%
Line 5	99 m	190°	180°	10°	1.52%
Line 7	99 m	175°	165°	10°	1.52%
Line 8	72 m	180°	180°	0°	0%
Line 9	99 m	90°	86°	4°	0.24%
Line 10	81 m	180°	180°	0°	0%
Line 11	81 m	110°	74°	36°	23.6%
Line 12	81 m	150°	152°	2°	0.06%
Line 13	72 m	150°	172°	12°	2.23%
Line 14	81 m	45°	35°	10°	1.54%
Line 15	99 m	145°	165°	20°	6.42%

Field Results and Observations

General Trends

The average velocity of the upper 15 m is approximately 175 m/s, consistent with the unconsolidated/alluvial sediment expected in this area and with the downhole data acquired in well 15B in January 2023. The velocity gradient at 15 m coincides with the interface between the unconsolidated sediment and shale bedrock. Average depth of investigation was 50-60 m across all lines as a result of surface wave frequencies generally above 4 Hz—lower frequencies would have resulted in deeper sampling depths. Dispersion curves were obtained using varying spread lengths for each line, ensuring that surface wave dispersion patterns at low frequencies were not distorted. Using the shortest optimal spread length on each line resulted in high lateral resolution and spatial extent of the resulting 2-D profiles while maintaining dispersion patterns at lower frequencies.

Line 1

Line 1 (Figure 7) is a slightly curved NW-E oriented line that extends across wells 8A, 10B, 11B, 44, 17, 42, 23B, and 41 (Table 3). Longer spread lengths were used than in 2021, resulting in the loss of imaging around well 41. Line 1 is the only line in this deployment with nonlinear receiver alignment. Two different source files were used to process the line, one with an azimuth of 120 degrees and the other 180 degrees. The depth of investigation was between 45 and 60 m, which is consistent with the 2021 survey. Variations in overtone image amplitudes were observed on this line in as few as 30 stations (Figure 8). The overtone image for station 1174 has strong fundamental mode energy between 4.5 Hz and 8 Hz. At station 1073, however, the fundamental mode becomes less coherent due to noise at higher frequencies. However, the dispersion curve trends are similar, and therefore the velocity profile is as well.

Table 3. Wells and corresponding station numbers across line 1.

Well	8A	10B	11B	44	17	42	23B	41
Station No.	1033	1086	1105	1136.5	1152.5	1196	1223.5	1265

Overall, the bulk-velocity trend observed in March 2023 is generally consistent with the past three years' results. A halo anomaly at well 8A observed in 2020 (dashed circle in Figure 7b) persisted relatively unchanged in 2021 and 2023 (Figure 7c). An area of elevated velocities between wells 17 and 42 observed in 2020 is more uniform with only subtle velocity halos near these wells. The velocity variation across line 1 is relatively minimal and all identified anomalies are within the bounds of native material.

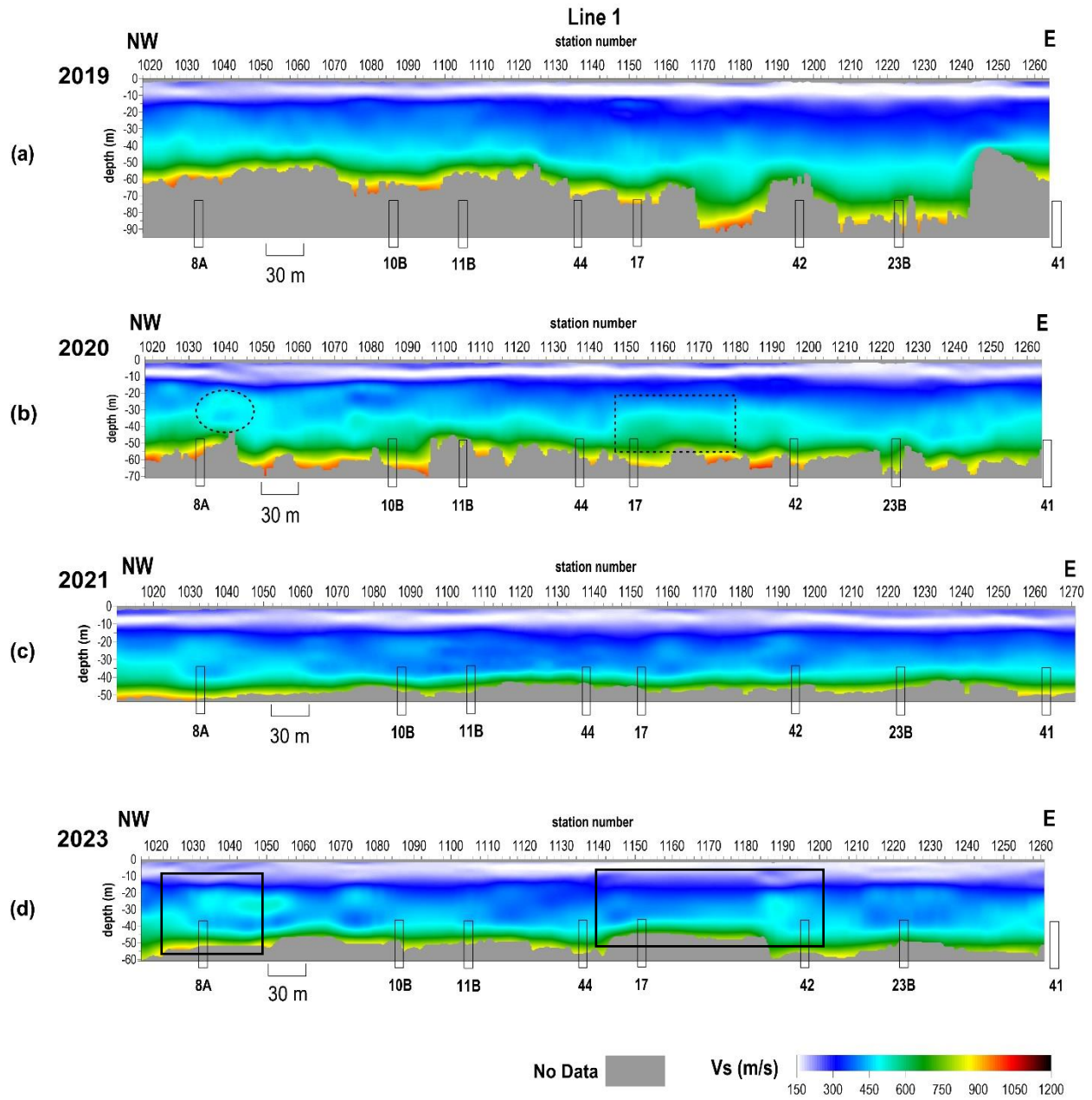


Figure 7. Shear wave velocity profiles from line 1 from (a) December 2019, (b) November 2020, (c) November 2021, and (d) March 2023.

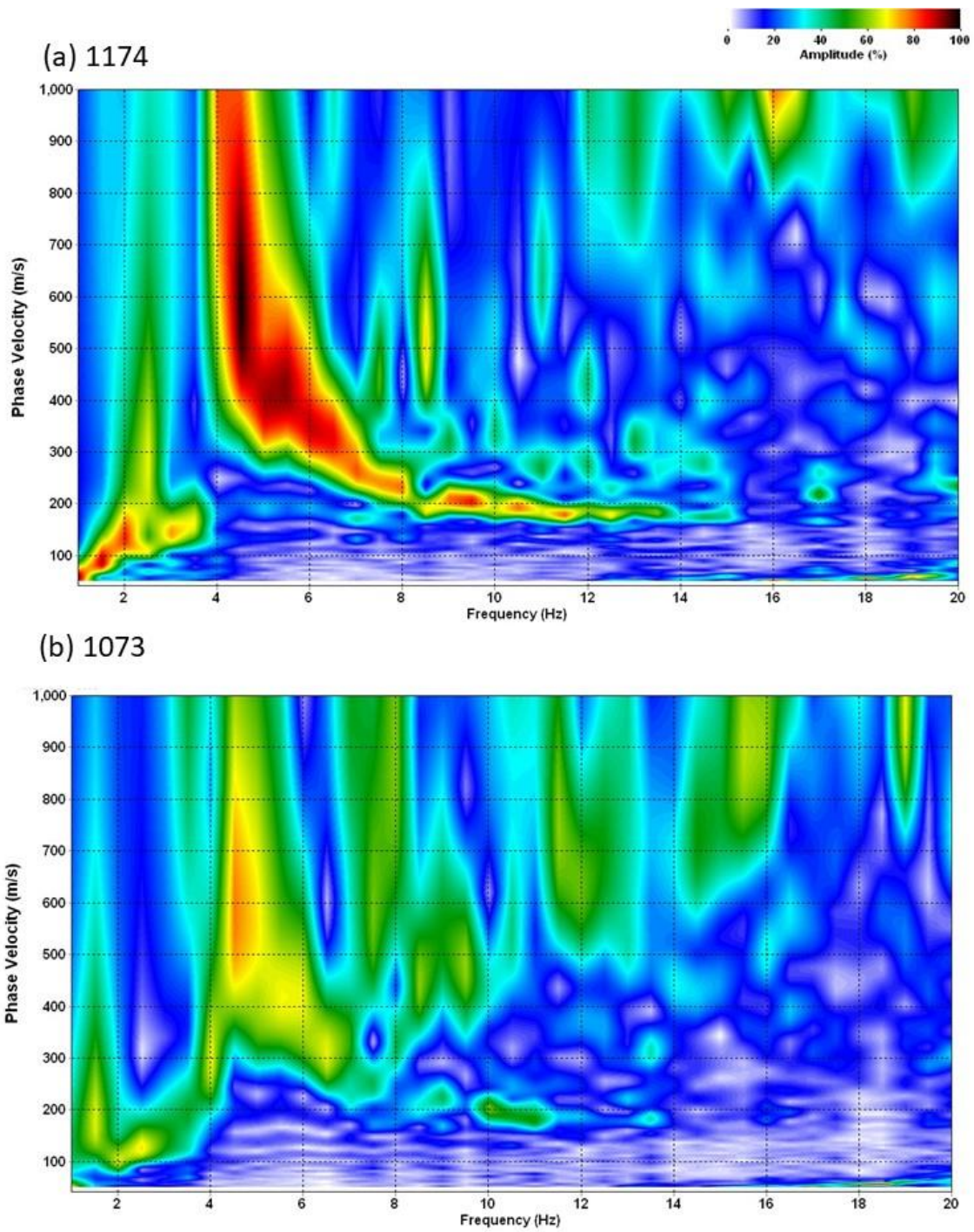


Figure 8. Changes in dispersion curve amplitude and coherency along line 1.

Line 3

Line 3 (Figure 9) is oriented W-E and extends over wells 46, 45, 22A, 23, 29, 30, 39, and 92 (Table 4). Two source records were used to maintain strong signal from 4 to 8 Hz along the line. The general bulk velocity profile remains consistent with past studies. A relatively subtle increase in velocity is observed near well 22A extending westward toward well 45, similar to the November 2020 survey (Figure 9b,d). The velocity profiles near well 92 (stations 3215-3240) are somewhat variable from year to year and may be associated with redistribution of stress in the overburden due to localized failure. Overall, 2023 results are similar to 2021 and within the range expected for native bedrock.

Table 4. Wells and corresponding station numbers across line 3.

Well	46	45	22A	23	29	30	39	92
Station No.	3025	3057	3080.5	3124	3148	3183.5	3199	3230.5

Line 4

Line 4 is a W-E oriented line that crosses wells 90, 89, 88, and 87 at stations 4044, 4076, 4107.5, and 4139.5, respectively (Figure 10). Two source records and longer spread lengths were used to maintain strong signal from 4.5 to 8 Hz along the line. Longer spread lengths resulted in limited spatial coverage at well 87, but still allow for assessment of conditions near this well. The bulk velocity trend for 2023 is consistent with past years and laterally consistent across the line, which suggests normal geologic conditions.

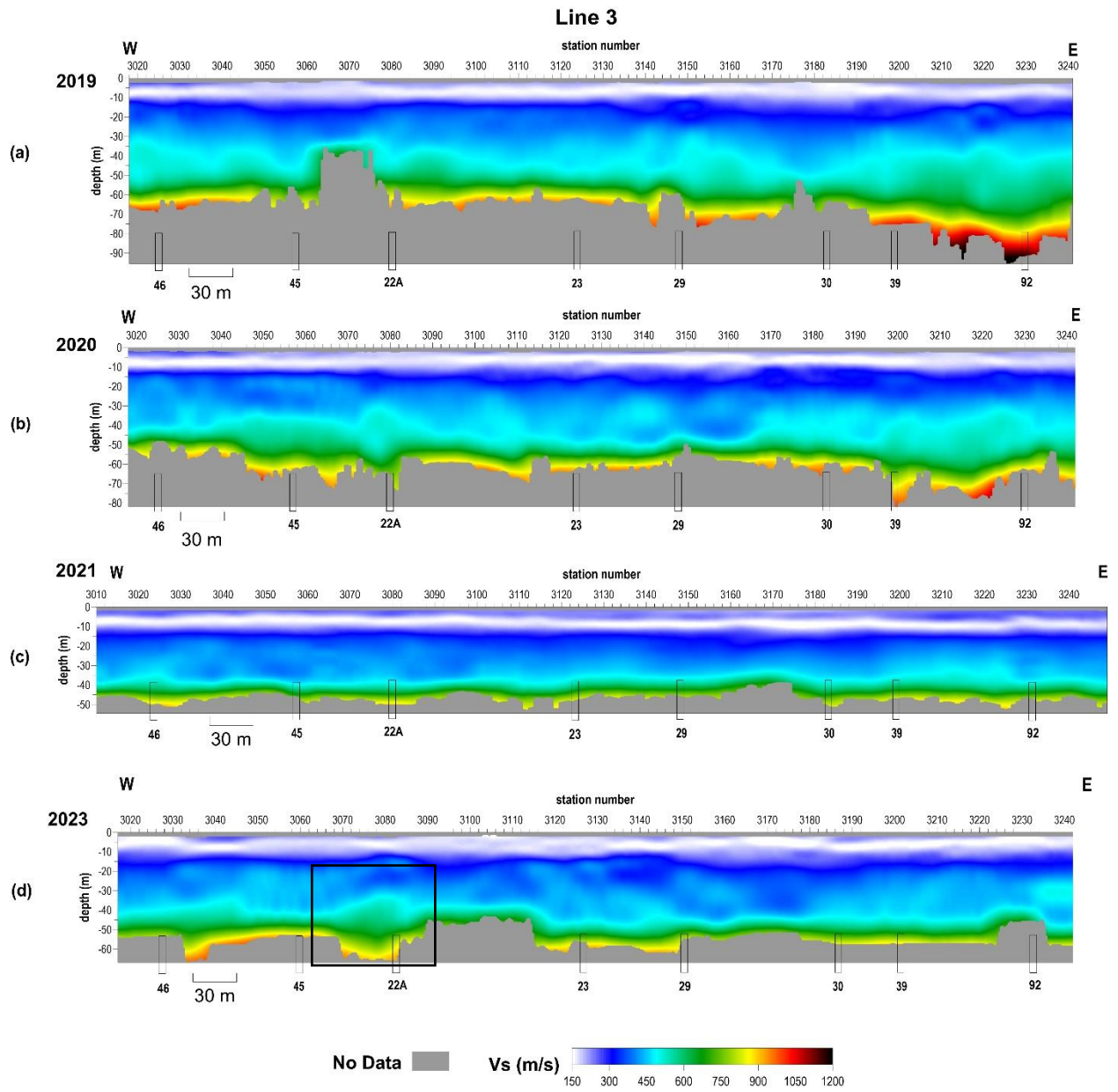


Figure 9. Shear-wave velocity profiles from line 3 from (a) December 2019, (b) November 2020, (c) November 2021, and (d) March 2023.

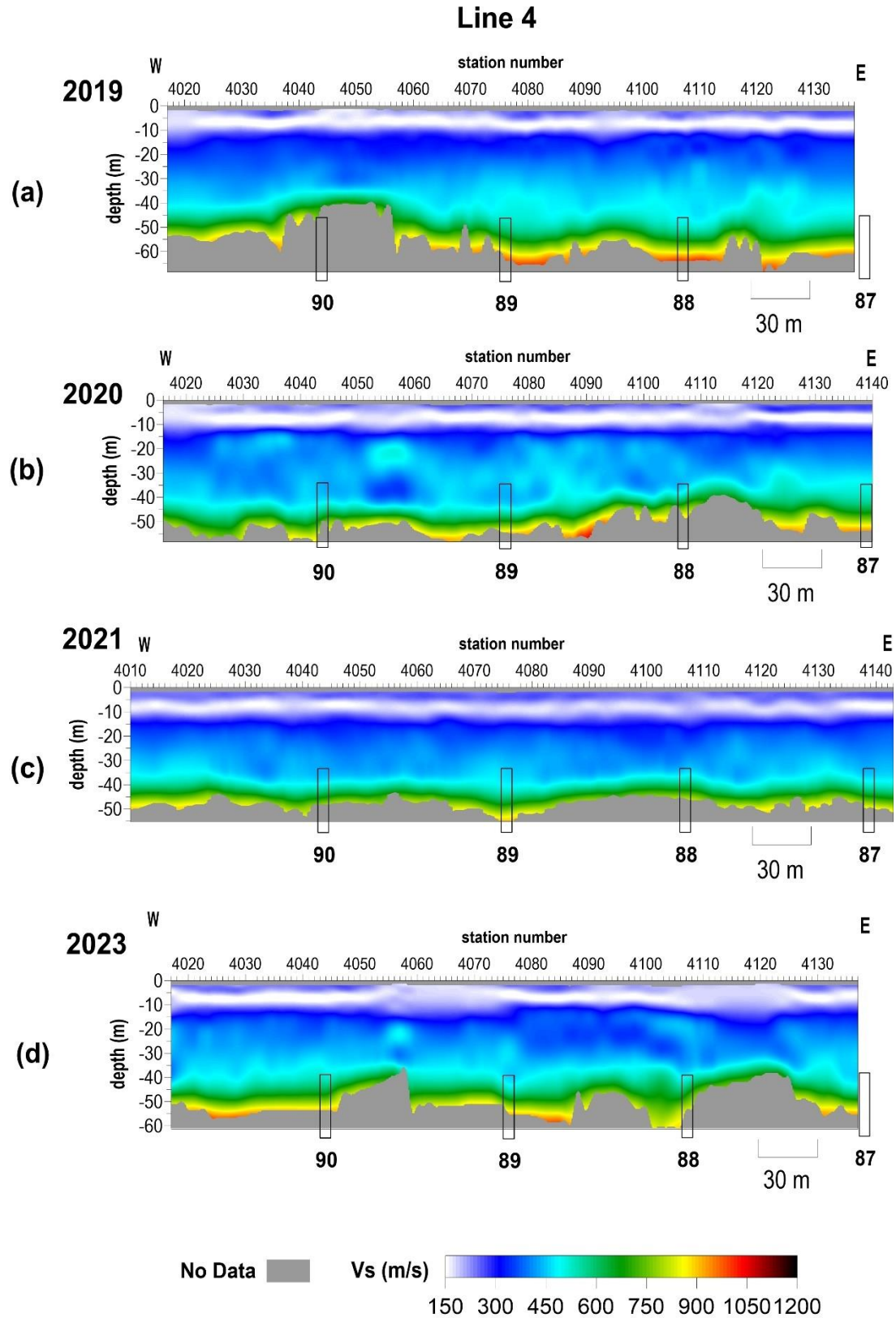


Figure 10. Shear-wave velocity profiles from line 4 from (a) December 2019, (b) November 2020, (c) November 2021, and (d) March 2023.

Line 5

Line 5 is oriented W-E and crosses wells 4B, 2B, 12B, and 14B at stations 5027.5, 5061, 5094, and 5126.5, respectively (Figure 11). A ~30-m-wide dome-shaped area of elevated velocity is observed near well 14B. Subtle anomalous velocity trends have consistently been observed near this well in previous years, possibly suggesting dynamic conditions. An area of apparent velocity decrease at the top of bedrock between stations 5100-5115 (dashed box in Figure 11) appears to be a result of uncertainty due to reduced S/N rather than a true velocity decrease or disturbed bedrock.

Line 7

Line 7 is oriented NW-SE and crosses over wells 8B, 15B, and 18 approximately located at stations 7028, 7073, and 7114, respectively (Figure 12). Well 15B has a history of dynamic shear-wave velocity (see Figure A-1 in the appendix). An area of elevated velocity at depth centered on well 15B was observed in 2015. Velocity decreased in 2017 and again in 2018, returning to velocities expected for normal conditions/stress. Velocity profiles in 2020 were somewhat anomalous but returned to normal conditions consistent with the rest of line 7 in 2021. In the present study, overall bulk velocity remains relatively consistent across the line compared to previous studies and is consistent with the native material. The depth of investigation was slightly greater in 2023 than 2021 due to an increased spread length used to generate dispersion curves. Apparent velocities on the west half of the line between wells 8B and 15B are about 15% higher than the east half of the line. Close examination of dispersion curves indicates some higher mode interference on the east half of the line, where there is greater uncertainty picking dispersion curves. A ~30 m wide somewhat dome-shaped area of elevated velocity about 10 m west of well 18. This is likely a result of higher mode interference and dispersion curve uncertainty.

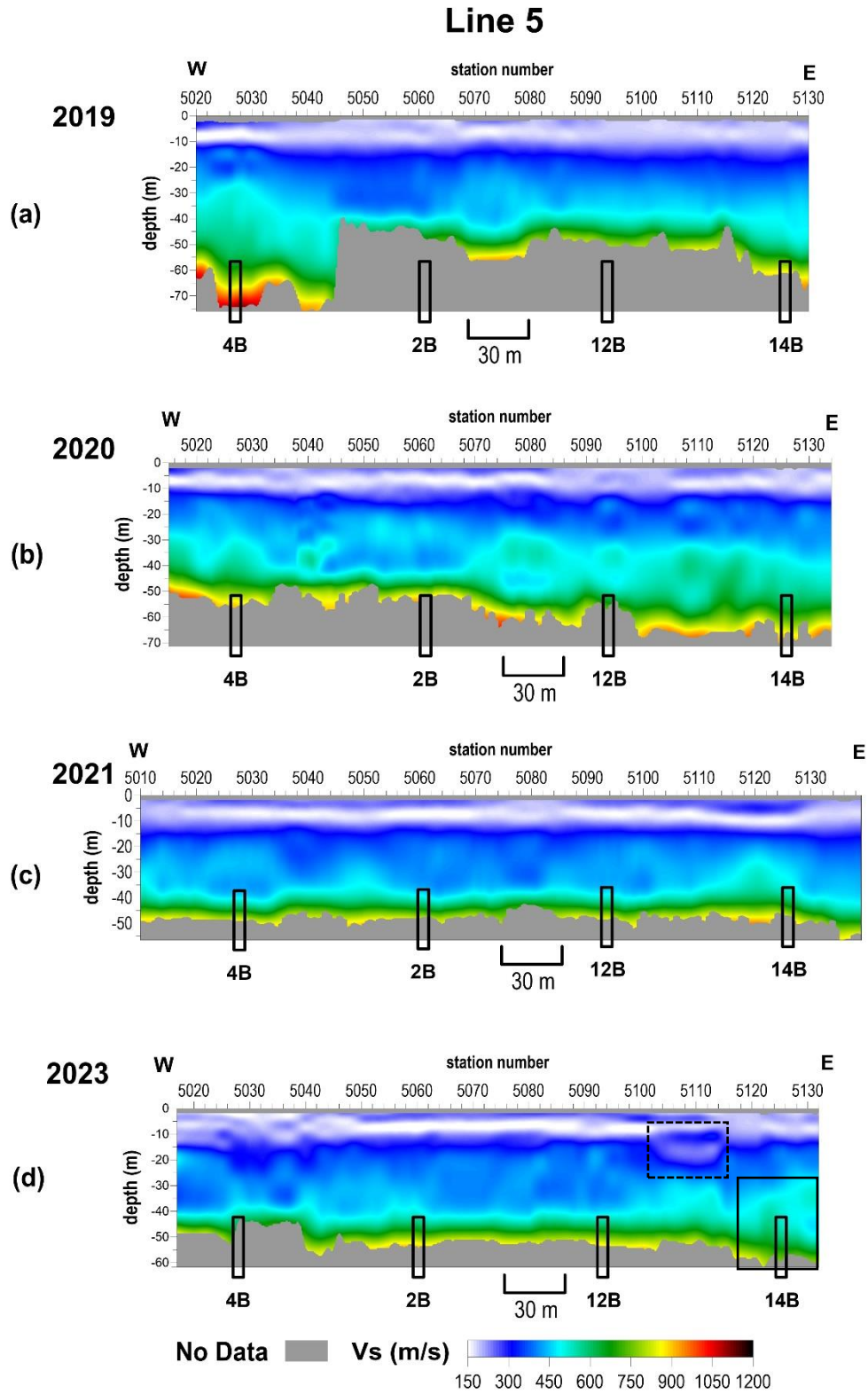


Figure 11. Shear-wave velocity profiles from line 5 from (a) December 2019, (b) November 2020, (c) November 2021, and (d) March 2023.

Line 7

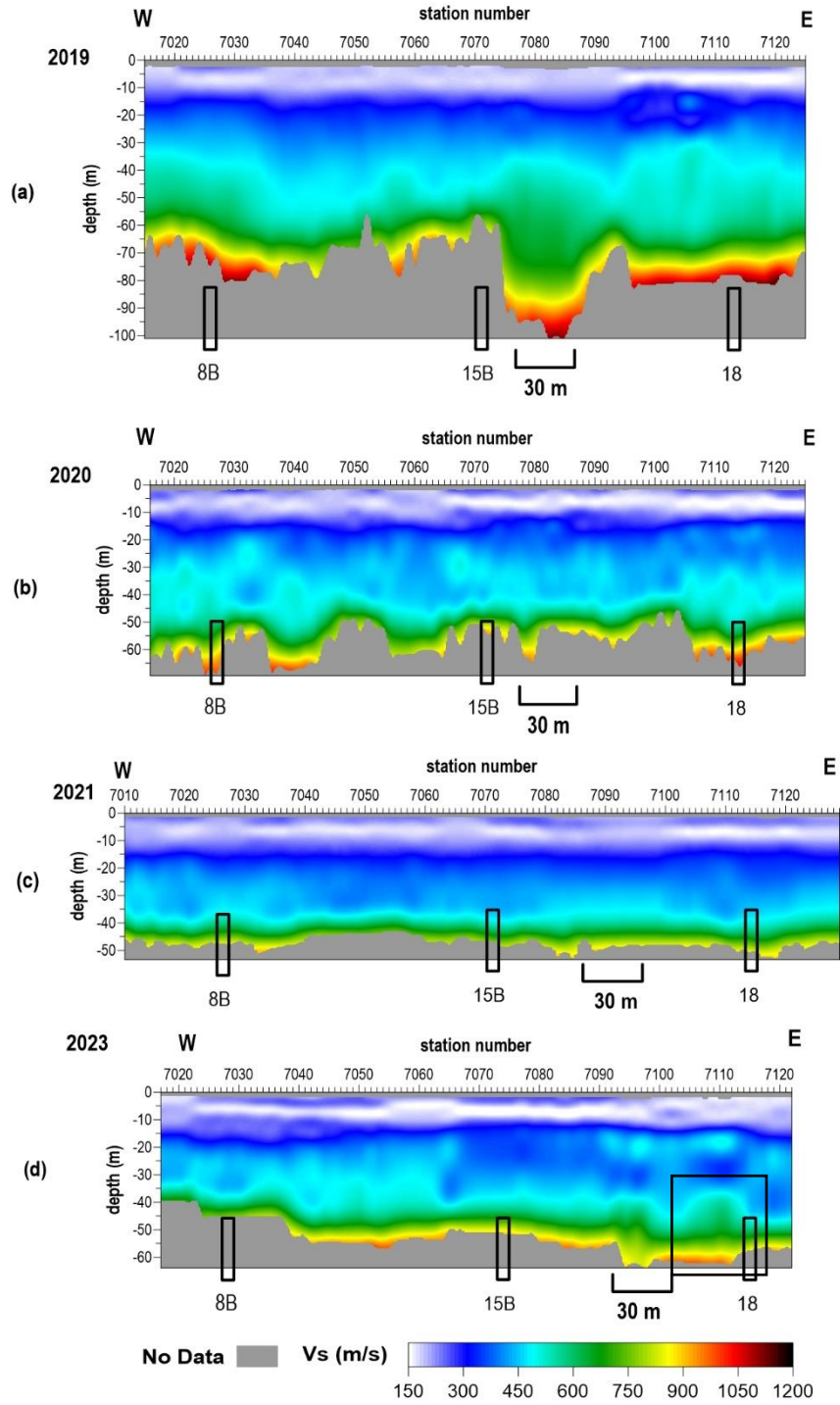


Figure 12. Shear-wave velocity profiles from line 7 from (a) December 2019, (b) November 2020, (c) November 2021, and (d) March 2023.

Line 8

Line 8 is oriented W-E and intersects well 13B at station 8025 (Figure 13). Four westernmost stations on line 8 extend across the paved entry road at the CBRA; these four stations (8008-8011) required rock plates rather than steel spikes to couple sensors to the ground surface. The bulk velocity profile in 2023 is consistent with previous year's results. Somewhat dynamic velocities have been observed at well 13B in the past few years. Velocity was elevated in 2018 and returned to normal representative stress conditions in 2019. A minor velocity inversion was observed in 2020, and conditions again appeared normal in 2021 and 2023. These timelapse observations may reflect periodic failure and associated changes in stress.

Line 9

Line 9 is a N-S oriented line that runs parallel to Williams Street and crosses wells 52, 53, 59, and 60 at stations 9031, 9061, 9098, and 9127, respectively (Figure 14). Well 60 had complete coverage last year, but due to a longer spread size, had slightly reduced coverage this year but still extends over all four wells. The overall bulk velocity trend in 2023 is different from 2021, with an apparent decrease in velocity on the north half of the line. Rather than a lateral change in stress, this is likely caused by lower S/N on the north end of the line and improved resolution of the fundamental mode dispersion curve on the south end of the line.

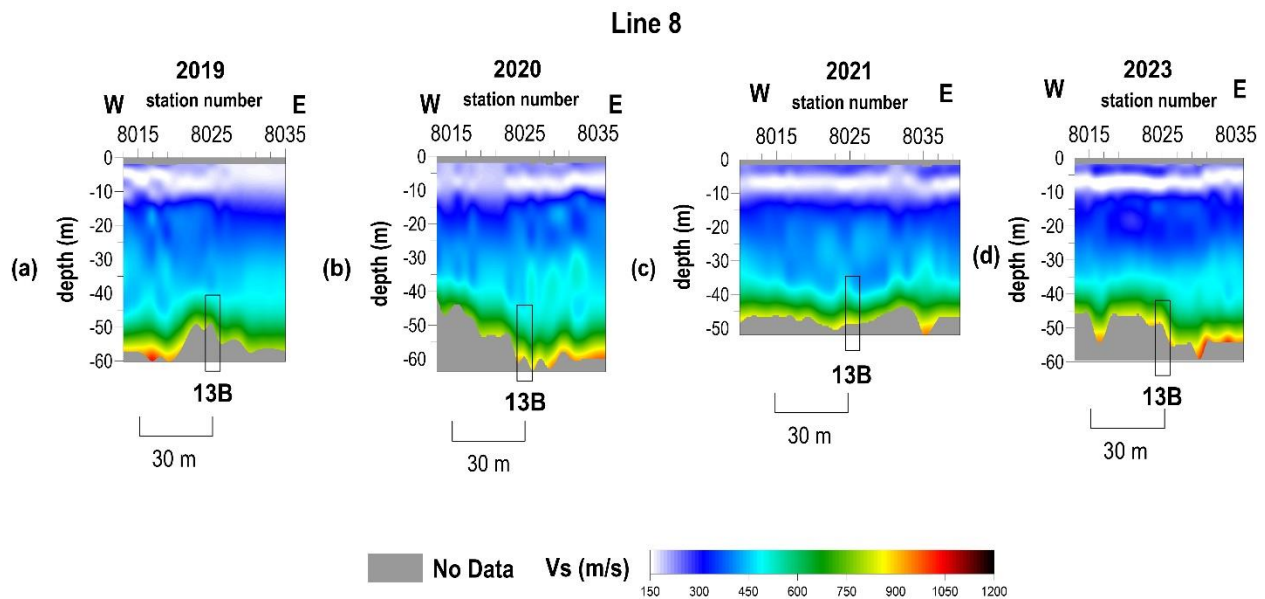


Figure 13. Shear-wave velocity profiles from line 8 from (a) December 2019, (b) November 2020, (c) November 2021, and (d) March 2023.

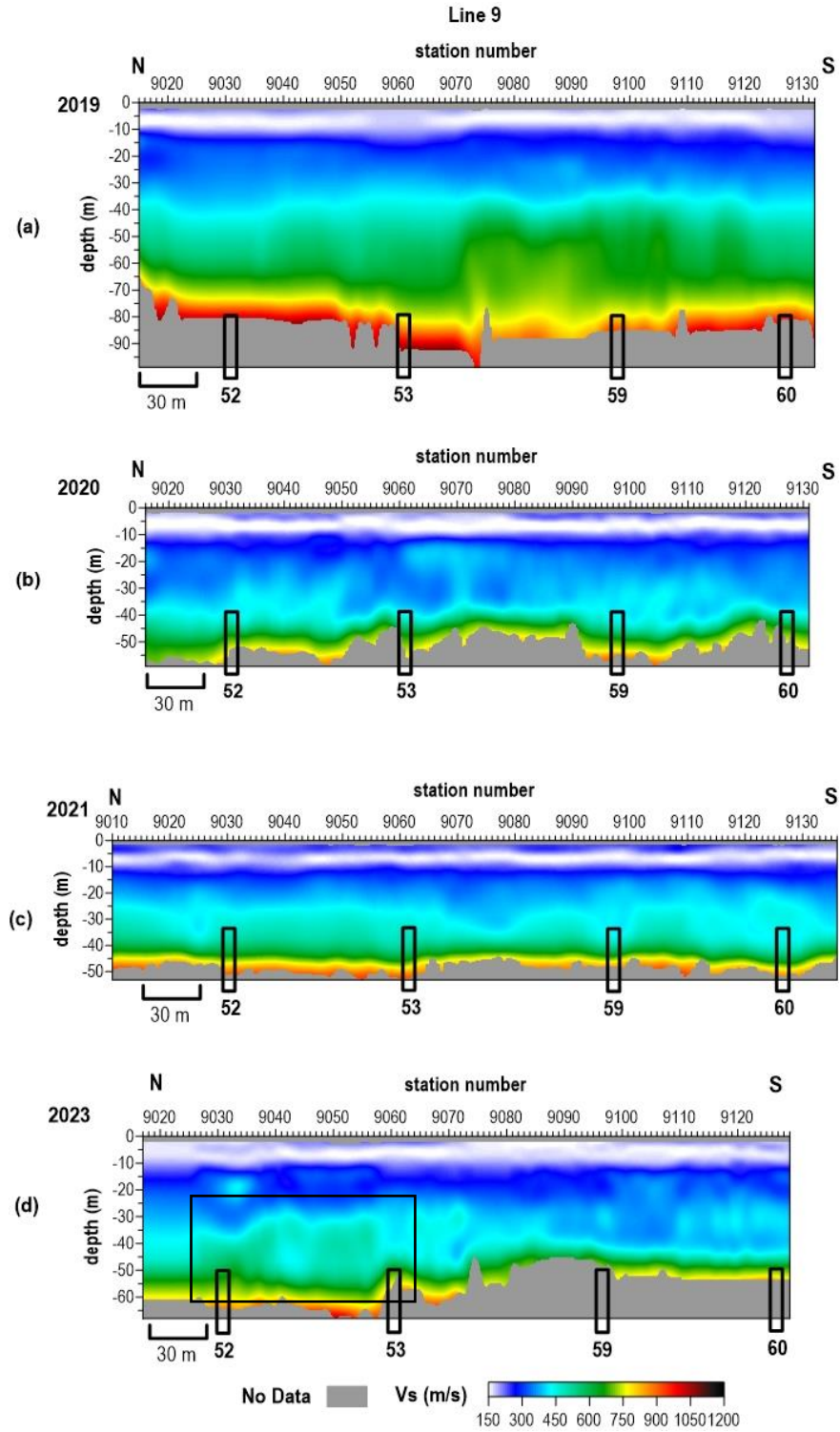


Figure 14. Shear-wave velocity profiles from line 9 from (a) December 2019, (b) November 2020, (c) November 2021, and (d) March 2023.

Line 10

Line 10 is a W-E oriented line that crosses well 2A at station 1022.5 (Figure 15). The westernmost 5 geophones are located on the road used to access the grain elevator and utilized rock plates instead of steel spikes. Timelapse changes observed at well 2A since 2013 suggest periods of elevated stress/velocity, subsequent roof rock failure and reduced overburden strength, and periods of relative stability (see Figure A-2 in the appendix). Between the May 2015 and November 2017 surveys, velocity in the overburden at well 2A increased slightly (~15%) and was consistent with native bedrock velocity. This suggests the void at that time was in a state of relative stability or consumed due to bulking with only gradual changes in stress. Multiple mode behavior was noted west of well 2A in 2020 suggesting heterogeneity at deeper depths where multiple stress states may have existed within the shale bedrock, and a period of relative stability in 2021. Overall, the bulk-velocity trend of the 2023 result is similar to 2021, or perhaps slightly elevated at ~ 35 m depth.

Line 11

Line 11 is oriented N-S over well 2A at station 1124 and well 4B at station 1151 (Figure 16). Multiple source records were used to maintain consistent signal throughout the line and corrections were applied to the final results to account for the difference in azimuth between the source and line. The average velocity below 30 m decreased 15% across line 11 from 2019 to 2020. Because such a corresponding decrease was not observed on nearly perpendicular line 10, the velocity variation in 2020 was azimuthal, which may be associated with changes in material strength. In 2023, velocities are similar to 2020, possibly suggesting azimuthal anisotropy and changes in material strength.

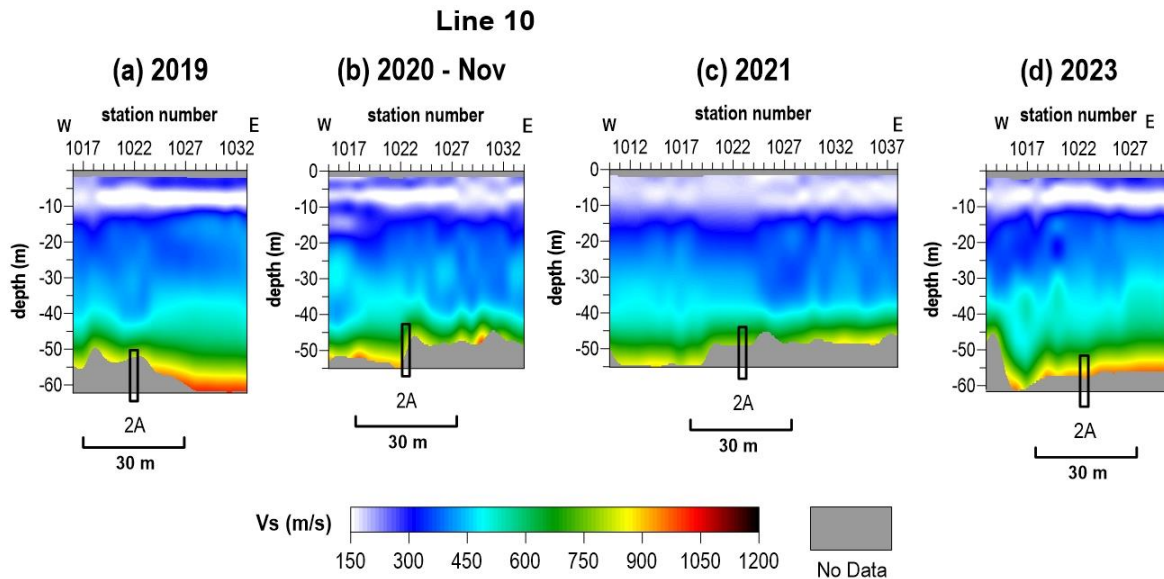


Figure 15. Shear-wave velocity profiles from line 10 from (a) December 2019, (b) November 2020, (c) November 2021, and (d) March 2023.

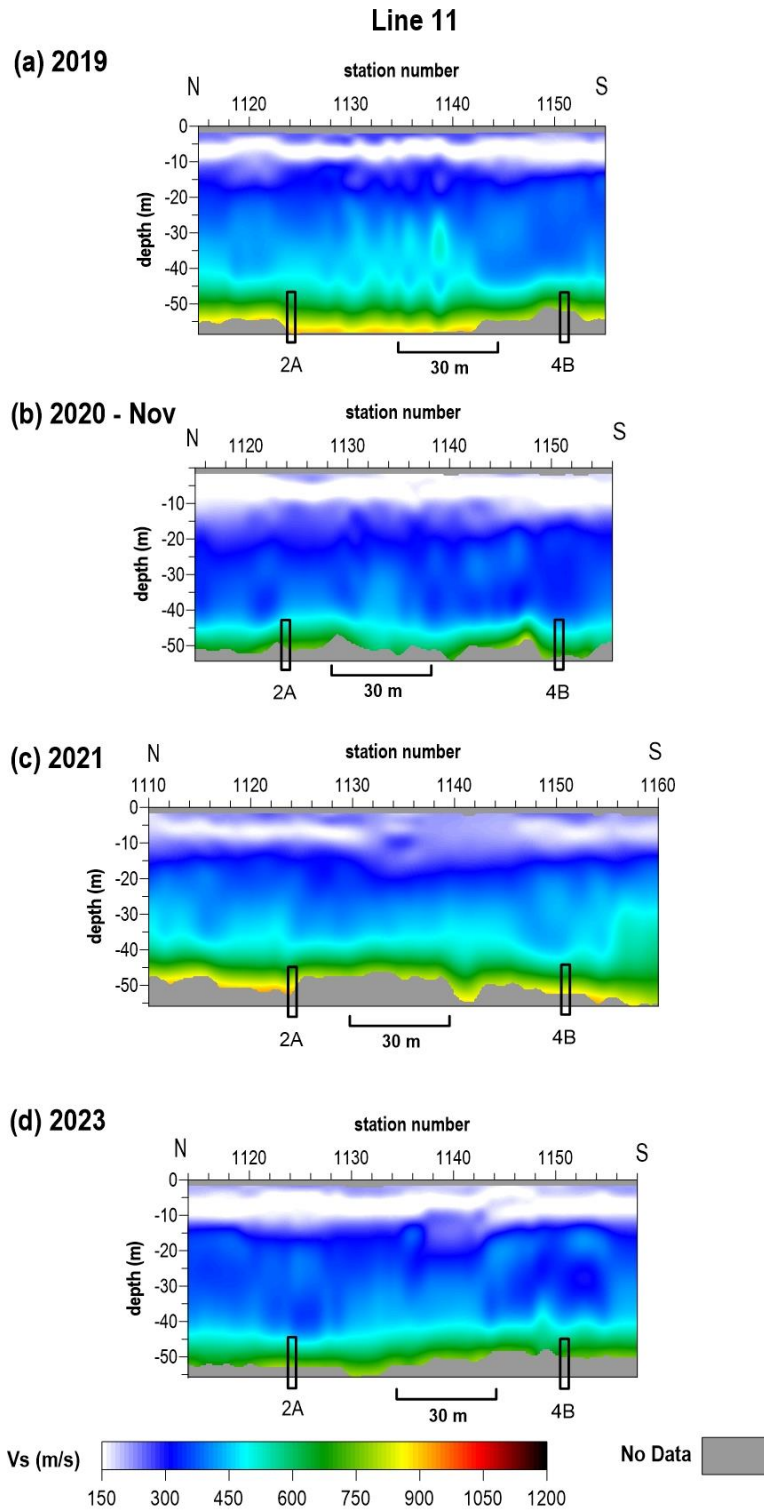


Figure 16. Shear-wave velocity profiles from line 11 from (a) December 2019, (b) November 2020, (c) November 2021, and (d) March 2023 investigation with approximate locations of well 2A and well 4B.

Line 12

Line 12 is a W-E oriented line that crosses wells 6B and 7B at stations 1238 and 1219, respectively (Figure 17). An approximately 25% velocity increase was observed in 2020 compared to previous years but was still within the range of bedrock velocity estimates on other lines at the CBRA and may have been a result of higher mode interference with the fundamental mode. Bulk velocities in 2021 returned to normal and are similar in 2023 but with a subtle dome-shaped area of elevated velocity in proximity to well 7B. These velocities are still within the expected range for bedrock at this site, but may suggest elevated velocity and possibly stress at 7B. It is possible apparent velocity is higher due to uncertainty in dispersion curve picks due to reduced S/N at corresponding frequencies. It does not represent a concern at this time, and continued monitoring will provide insight into the cause of the apparent velocity increase.

Line 13

Line 13 is oriented W-E and intersects wells 7A and 4A located approximately at stations 1328 and 1376.5, respectively (Figure 18). The bulk velocity trend has remained relatively consistent since 2018. Velocities from 2023 appear to be very similar to 2021 with similar depths. Velocity values across this area are within normal range for native material and represent a normal stress regime. There is an indication of increased velocity between 7A and 4A, a feature worth tracking in future annual monitoring data sets.

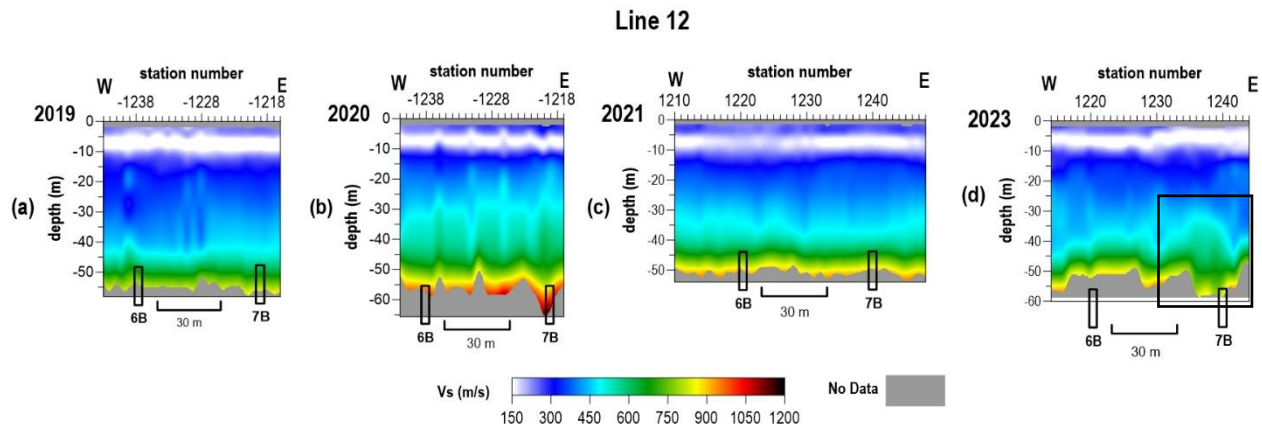


Figure 17. Shear-wave velocity profiles from line 12 from (a) December 2019, (b) November 2020, (c) November 2021, and (d) March 2023 investigation.

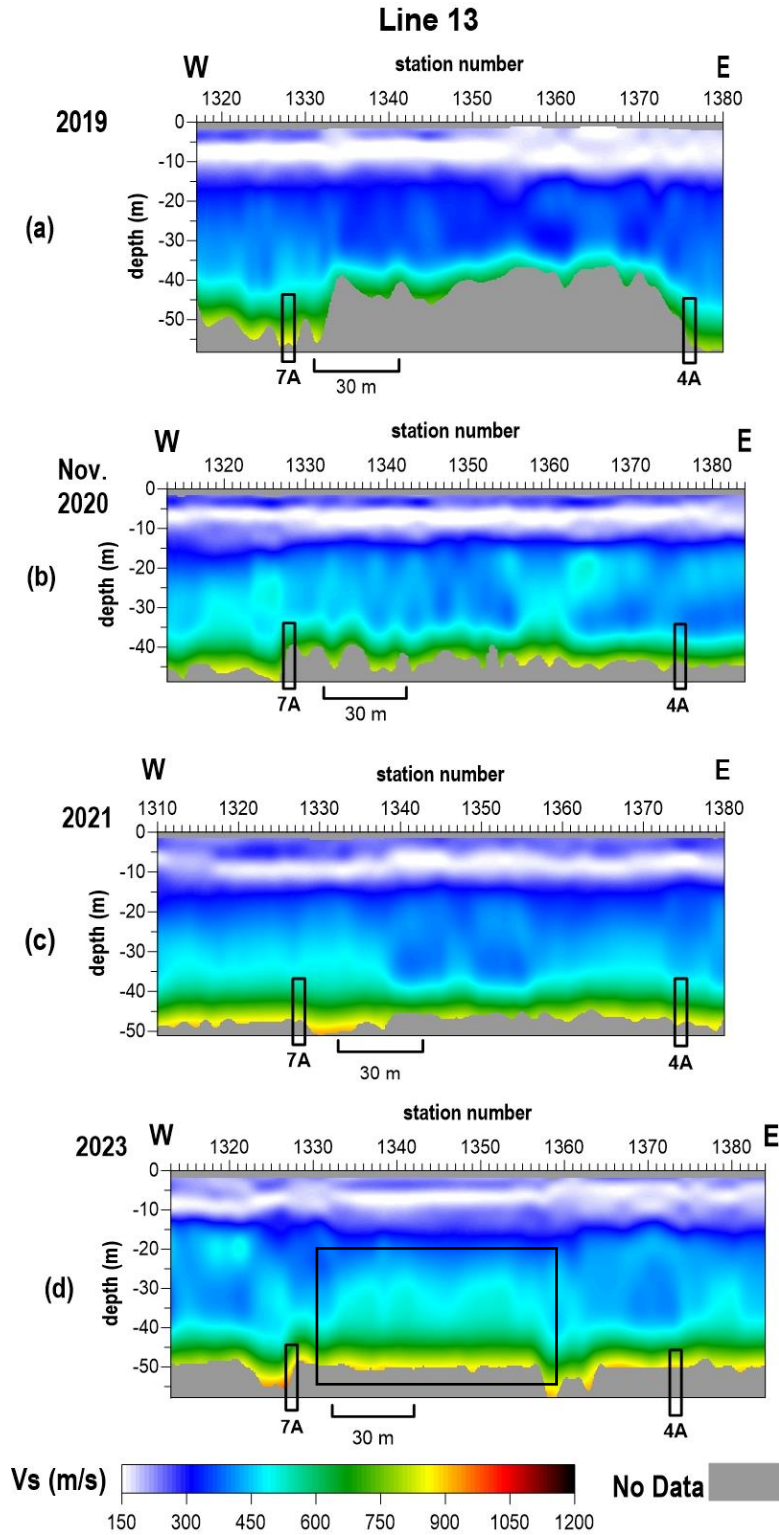


Figure 18. Shear-wave velocity profiles from line 13 from (a) December 2019, (b) November 2020, (c) November 2021, and (d) March 2023 investigation.

Line 14

Line 14 is oriented W-E and extends across wells 3B and 1B, which are approximately located at stations 1430 and 1450 respectively (Figure 19). The 2023 results are similar to the past two surveys, but with slight variation in the depth of investigation due to improved S/N at low frequencies near the east end of the line. An apparent pull down in the top of bedrock between stations 1035-1045 is likely a result of variability in the inversion layer model caused by the reduced investigation depth. Overall bulk velocity profiles suggest a normal stress regime.

Line 15

Line 15 is orientated NW-SE over wells 19, 20, 25, 26, 33, 36, and 94 (Table 5). This line was a new addition to the passive monitoring survey in 2021 and spans a portion of a 2-D profile recorded during a 2010 passive surface wave survey. The overall bulk velocity trend in 2023 for line 15 (Figure 20) is largely consistent with the 2021 and 2010 surveys (Figure 21) with only subtle (~15%) variability. Considering the plugged status of the wells along the railroad tracks, the velocity profile between wells 25 and 94 represents normal variability in the estimated shear velocity from year to year.

In the 2023 survey, there is a subtle discontinuity near the top of bedrock at 20-25 m depth between wells 19 and 20. Dispersion curves for stations around the collapsed salt jug show lower and less coherent fundamental mode energy compared to stations where the receiver spread was fully away from the feature (Figure 22). Higher mode energy is observed in the overtone image near the collapse feature between 5.5 Hz and 6.5 Hz (Figure 22a). A representative dispersion curve where the spread is fully outside the surface expression exhibits a single fundamental mode trend that is coherent over relevant frequencies (Figure 22b). This multimode behavior supports the suggestion that multimode dispersion patterns may be an indication of heterogeneities at depth for wells over salt jugs that have not migrated to the surface. The apparent velocity discontinuity near the top of bedrock is likely a result of uncertainty in picking the fundamental mode due to the presence of the higher mode. This velocity variability is well within the range expected for natural variation and inherent uncertainty, suggesting a normal stress regime but a feature worth tracking from year to year.

Table 5. Wells and corresponding station numbers across line 15.

Well	19	20	25	26	33	36	94
Station No.	15025	15058	15080	15123	15138	15174	15207

Line 14

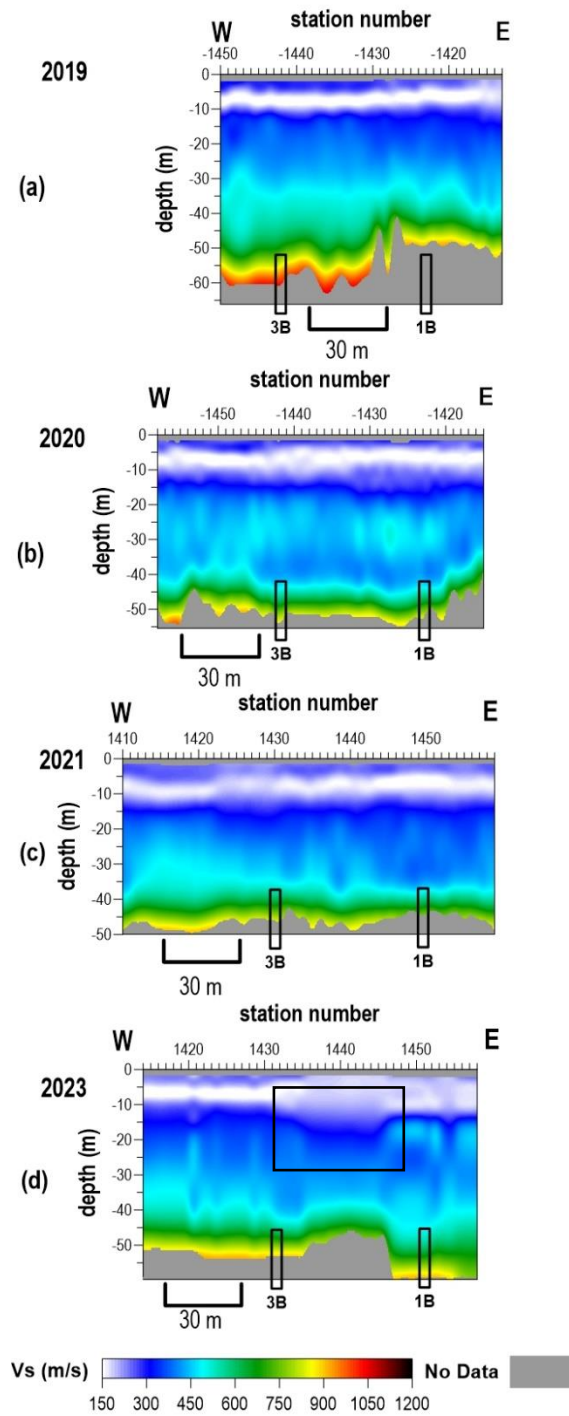


Figure 19. Shear-wave velocity profiles from line 14 from (a) December 2019, (b) November 2020, (c) November 2021, and (d) March 2023 survey.

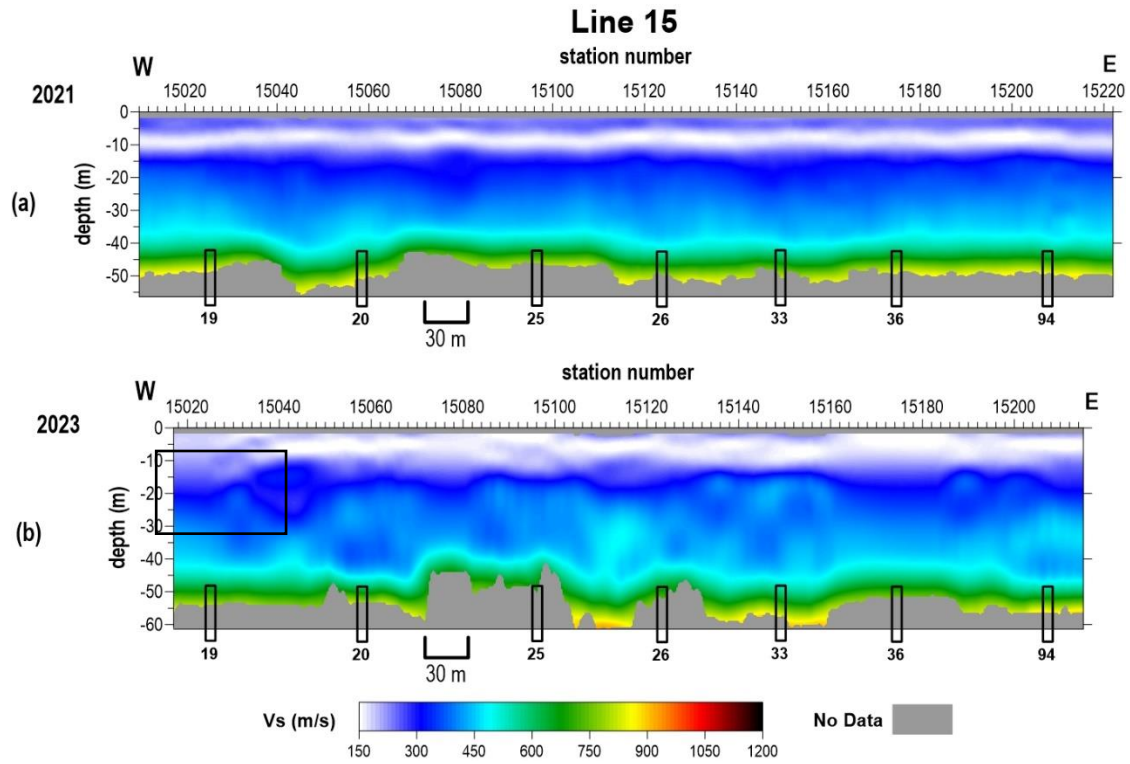


Figure 20. Shear-wave velocity profile from line 15 from (a) November 2021 and (b) March 2023.

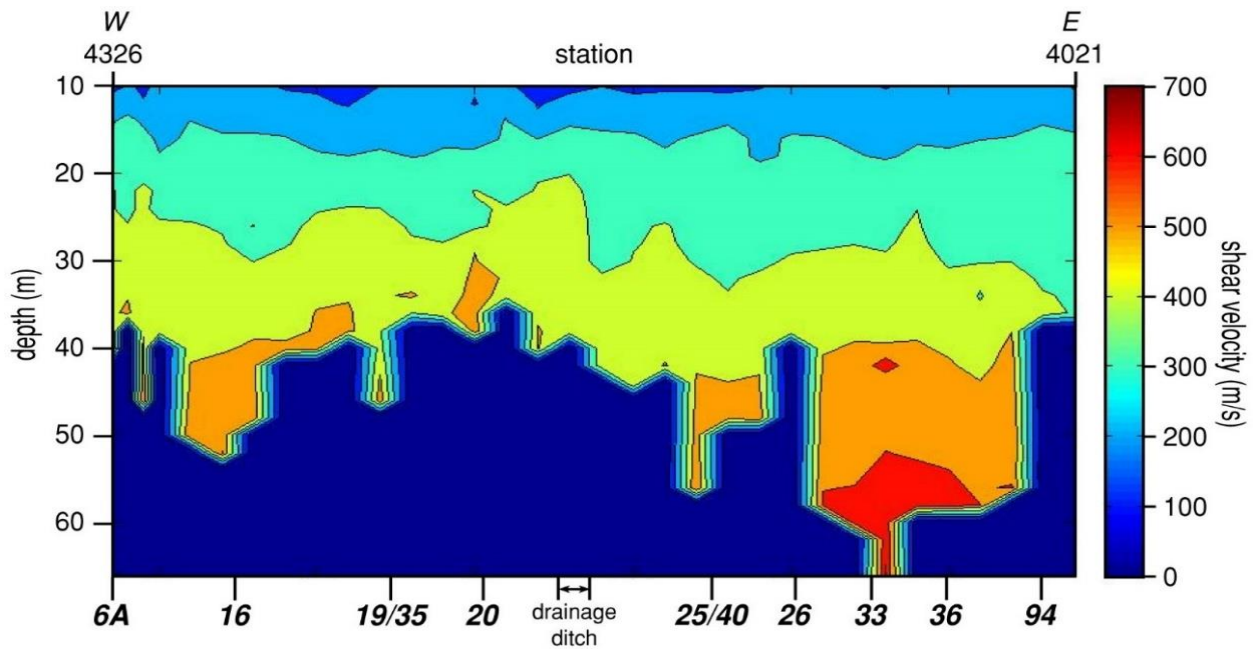


Figure 21. Shear wave velocity profile from the 2010 survey over the location of line 15 in the current survey.

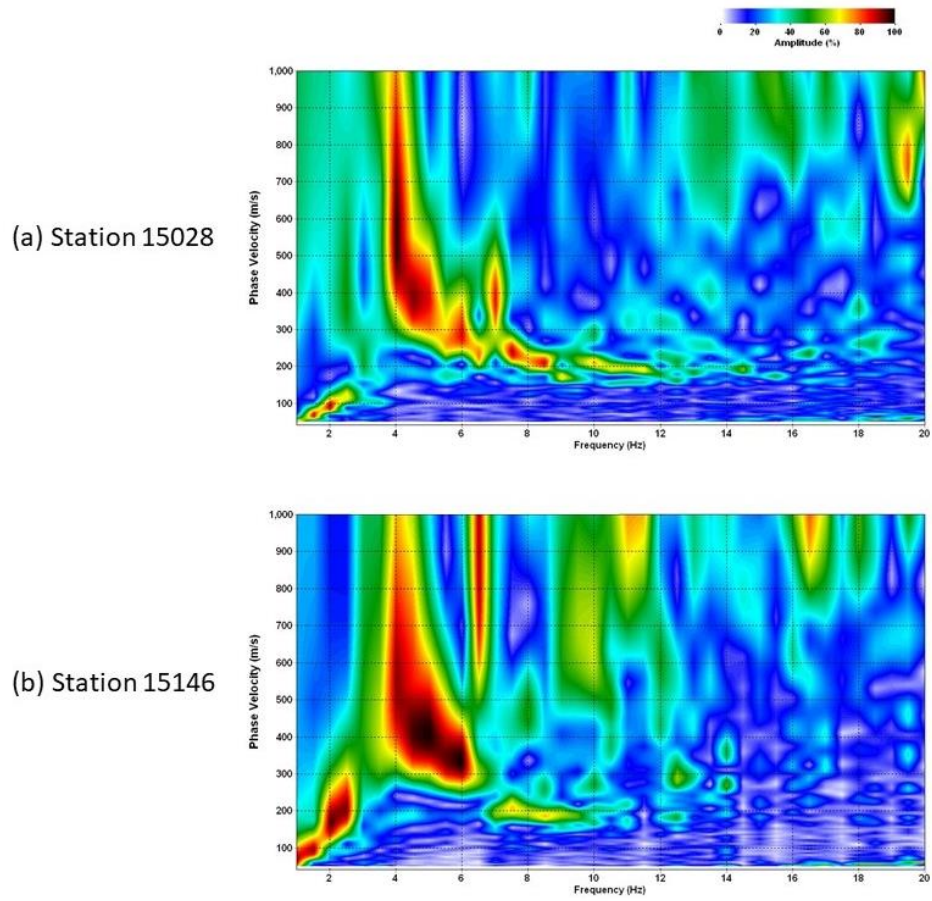


Figure 22. Representative dispersion curves (a) over low velocity anomaly and (b) towards the middle of line 15.

Interpretation and Discussion

Wells with conditions of normal stress regime and consistent surface-wave behavior

Wells 1B, 6B, 7B, 10B, 11B, 23, 23B, 25, 26, 29, 30, 33, 36, 39, 41, 44, 46, 87, 88, 89, 90, 92, and 94.

Wells with varied surface wave behavior, but interpreted as consistent with normal or currently stable stress regime

Wells 19 and 20 (line 15)

Dispersion curves around the collapse feature in proximity to wells 19 and 20 possess less coherent fundamental mode energy with higher mode interference compared to stations where the receiver spread was fully away from the feature. This multimode behavior supports the suggestion that multimode dispersion patterns may be indicative of heterogeneities at depth for wells over salt jugs where the void has not migrated to the surface. These characteristics are consistent between 2021 and 2023, suggesting an overall stable stress regime along line 15.

Wells 3B, 4A, 7A, and 8B

Past reports have called out these wells for having attenuated fundamental mode energy and corresponding limited depth of investigation. Depths across these wells were more consistent with surrounding stations on 2021 data. Nonetheless, bulk-velocity trends acquired over these wells likely represent natural geologic conditions with a normal stress regime. In 2023, the depth of investigation decreased slightly at 8B (line 7) and between wells 3B and 1B (line 14), and slightly elevated velocity between wells 7A and 4A (line 13), which need to be monitored in future surveys.

Wells 13B, 15B, and 18

Velocity at well 13B (line 8) was elevated in 2018, reduced to expected bedrock velocity in 2019, and slightly elevated in 2020, reduced in 2021, and has variable depth of investigation in 2023. Although the velocity and surface wave characteristics near this well remain variable, these changes do not appear to represent imminent vertical migration. Elevated velocity at depth and associated increase in depth of investigation near well 15B (line 7) prompted a midyear monitoring survey in August 2020. Subtle variability at neighboring well 18 (line 7) has persisted since 2019, with a minor dome-shaped elevated velocity in 2023. Timelapse observations suggest dynamic changes at these wells that could be related to variations in roof rock properties, however, subsurface conditions at the time of the 2021 and 2023 surveys appear stable.

Wells 17, 22A, 42, and 45

An area of elevated velocity was observed between wells 17 and 42 (line 1) and 45 and 22A (line 3) in 2020. In 2021 and 2023, the overall velocity trend was more consistent with 2019, with a more uniform profile between wells on lines 1 and 3 with only subtle velocity hallos near wells 17 and 42. A 30 m dome-shaped area of elevated velocity observed near well 22A is observed in 2023 and is worth monitoring in future surveys. In general, these observations are consistent with the dynamics these wells have demonstrated in years past.

Wells 2B, 12B (line 5)

A subtle halo anomaly was observed between wells 2B and 12B in 2020. The velocity profile between these wells returned to baseline bedrock velocity in 2021 and remains so, indicating normal geologic variations. Timelapse observations along line 5 over the past few years suggest dynamic stress changes possibly associated with changes in the roof structures/characteristics of salt jugs at these wells have occurred, but wells 2B and 12B appear to currently be in a period of relative stability.

Well 8A (line 1)

The halo anomaly first observed over well 8A in 2018 has persisted since 2020. The relative magnitude, depth, and shape of this anomaly has remained consistent throughout this time. The velocity is within the bounds of native material, but due to its apparent absence in 2019, it may be an indicator of dynamic processes at depth and currently elevated but stable stress in the bedrock at well 8A.

Wells with possibly varying stress regime

Wells 2A and 4B

Similar to previous years, in 2023 multi-mode dispersion curves were observed near well 2A along line 10, potentially indicative of heterogeneity below the imaging depth of these data. Velocity on line 10 is similar to the previous few years, and possibly slightly elevated between 30-50 m. Line 11 intersects wells 2A and 4B. In 2020, azimuthal variation in bedrock velocity was noted between lines 10 and 11 with a relative 15% decrease in velocity on line 11. Similar azimuthal velocity variation is again observed in 2023. These timelapse changes across lines 10 and 11 suggest the possibility of dynamic stress changes.

Wells 14B (line 5)

A dome-shaped area of elevated velocity appeared west of well 14B in 2021. Although velocity returned to normal at this location in 2023, the velocity at well 14B is slightly elevated and there is a subtle velocity halo east of well 14B. Timelapse observations at this well over the past few years suggest dynamic stress changes possibly associated with changes in the roof structures/characteristics of the salt jug has occurred.

Wells 52, 53, 59, 60 (Williams Street)

The velocity gradient in the upper 30 m of the Williams Street line (line 9) has been reasonably consistent since the beginning of timelapse passive surface wave monitoring. Velocity trends below 30 m have varied slightly over time and have typically been elevated compared to other lines at the CBRA. In 2021, either shear stress or bedrock velocity has appeared higher along this line. In 2023, velocities below 30 m remain elevated on the northern half of the line (spanning wells 52 and 53) and decreased on the southern half of the line (spanning wells 59 and 60). These observations may suggest dynamic processes at depth (possibly localized failure and redistribution of stress at wells 59 and 60) and currently elevated stress in the bedrock on the northern part of the line.

The spatial distribution of wells categorized by timelapse surface wave behavior reveals some commonalities worth highlighting (Figure 23). In general, wells surveyed on the eastern half of the site have retained more consistent velocity profiles and surface wave characteristics with less timelapse variability. Although it is unclear why this is the case, there are more wells in this part of the site that are either newer, have been plugged, or are known to have failed and, therefore, represent a stable setting. Wells on the western half of the site are generally older. These observations could indicate that differences in construction techniques or production history between older and newer wells may have led to a difference in overall stability. Returning to the extensive review of production history, driller information, drill data, and construction techniques undertaken by Burns and McDonnell a decade or more ago may provide some insight into these observations.

Additionally, wells with the greatest variability (Williams Street, and 2A/4B near the Irsik & Doll grain elevator) are primarily surveyed using receiver lines oriented approximately N–S, whereas the remainder of the wells at this site are surveyed using lines oriented approximately E–W. Characteristics of N–S sources, proximity to anthropogenic activity (i.e., grain elevator and neighborhood), or some other attribute yet to be determined may play some role in this seeming disparity. It may also be coincidence, but that is unclear at this time and justifies continued study.

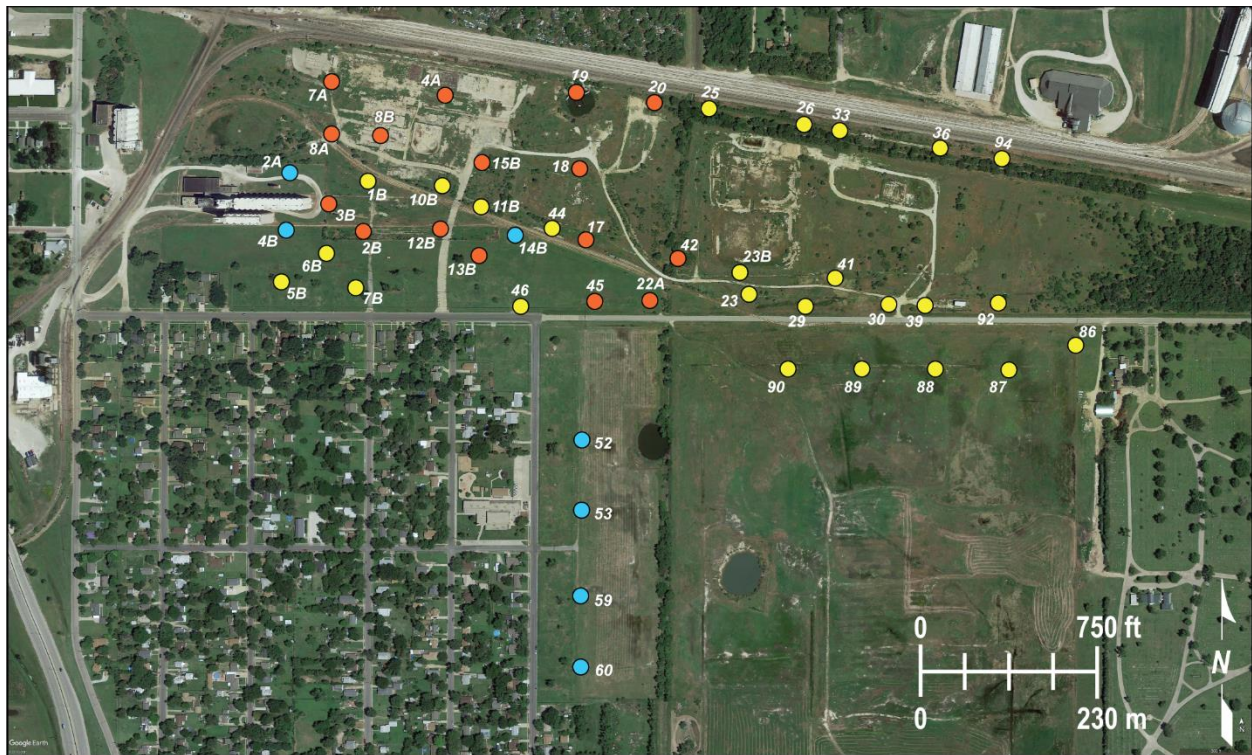


Figure 23. Wells at the CBRA categorized by surface wave characteristics.

Conclusions and Recommendations

The shear-wave velocity directly over or in proximity to the majority of wells in this 2023 study continues to represent natural geologic conditions and a normal stress regime. Shear-wave velocity profiles were classified into three different categories based on measurements and wave observations in overburden above and in proximity to each well: (1) normal stress regime and well-behaved surface wave propagation, (2) inconsistent surface wave behavior and normal or currently stable stress regime, or (3) changes in stress regime. Anomalous shear-wave velocity profiles from seven wells are sufficiently outside the normal range to justify a heightened awareness and focused monitoring on future surveys.

Drilling at the site provided unexpected and interesting discoveries associated with two jugs noted in previous passive seismic studies as possessing variable shear wave velocities and therefore changing stress field above the voids. The triple jug at well 2A was unexpected and with such a highly irregular geometry and 3 different roof spans, instability is likely and would result in both the anisotropic shear velocity and fluctuations from high to low stress as noted on previous monitoring surveys. Well 15B was drilled in a slightly offset hole, but within 10 ft of the original well. Penetration well into the upper 30 ft of the salt did not encounter a jug. Considering the shear velocity variability, one possible explanation is one or more connections between 15B and one of the wells to the south and west (10B and 11B). Active borehole surveys provided ground truth velocities that can be used to calibrate V_s from passive MASW. Initial analysis indicates that the phase velocities of dispersion curves more closely correlated with average V_s rather than interval V_s . Although MASW velocities are lower than the borehole velocities, absolute velocity is not necessary to assess stress conditions overlying the salt jugs and does not impact previous interpretations and an initial model based on borehole velocities can be used to calibrate MASW velocity profiles.

Strength characteristics estimated from shear-wave velocities that were derived from the passive MASW surveys around wells 2A and 4B (line 1); 14B (line 5); and 52, 53, 59, and 60 (line 9 along Williams Street) have changed from historical surveys and are consistent with possible increases in stress due to under-supported spans of roof rock above voids. Voids associated with these seven wells currently represent the only apparent potential threat of void migration toward the ground surface and thereby affecting the stability of material above the bedrock surface in the survey area. In general, since current conditions largely reflecting normal or stable stress regime with a few areas possessing subtle and relatively minimally elevated stress, we recommend continued monitoring on an annual basis with no apparent need this year for a well-specific interim survey.

References

- Davies, W.E., 1951, Mechanics of Cavern Breakdown. *Bulletin of the National Speleological Society*, no. 13, p. 36-43.
- Dellwig, L.F., 1963, Environment and mechanics of deposition of the Permian Hutchinson Salt Member of the Wellington shale: Symposium on Salt, Northern Ohio Geological Society, p. 74-85.
- Dvorkin, J., A. Nur, and C. Chaika, 1996, Stress sensitivity of sandstones: *Geophysics*, v. 61, p. 444-455.
- Eberhart-Phillips, D., D.-H. Han, and M.D. Zoback, 1989, Empirical relationships among seismic velocity, effective pressure, porosity, and clay content in sandstone: *Geophysics*, v. 54, p. 82-89.
- FLAC, 2005, Fast Lagrangian Analysis of Continua, version 7.0: ITASCA Consulting Group, Inc. Minneapolis.
- Holdaway, K.A., 1978, Deposition of evaporites and red beds of the Nippewalla Group, Permian, western Kansas: *Kansas Geological Survey Bulletin* 215.
- Ivanov, J., R.D. Miller, S.L. Peterie, J.T. Schwenk, J.J. Nolan, B. Bennett, B. Wedel, J. Anderson, J. Chandler, and S. Green, 2013, Enhanced passive seismic characterization of high priority salt jugs in Hutchinson, Kansas: Preliminary report to Burns & McDonnell Engineering Company.
- Khaksar, A., C.M. Griffiths, and C. McCann, 1999, Compressional- and shear-wave velocities as a function of confining stress in dry sandstones: *Geophysical Prospecting*, v. 47, p. 487-508.
- Kulstad, R.O., 1959, Thickness and salt percentage of the Hutchinson salt; *in* Symposium on Geophysics in Kansas: *Kansas Geological Survey Bulletin* 137, p. 241-247.
- McGuire, D., and B. Miller, 1989, The utility of single-point seismic data; *in* Geophysics in Kansas, D.W. Steeples, ed.: *Kansas Geological Survey Bulletin* 226, p. 1-8.
- Merriam, D.F., 1963, The Geologic History of Kansas: *Kansas Geological Survey Bulletin* 162, 317 p.
- Merriam, D.F., and C.J. Mann, 1957, Sinkholes and related geologic features in Kansas: *Transactions of the Kansas Academy of Science*, v. 60, p. 207-243.
- Miller, R.D., 2011, Progress report: 3-D passive surface-wave investigation of solution mining voids in Hutchinson, Kansas: Interim report to Burns & McDonnell Engineering Company, January, 9 p.
- Miller, R.D., J. Ivanov, S.D. Sloan, S.L. Walters, B. Leitner, A. Rech, B.A. Wedel, A.R. Wedel, J.M. Anderson, O.M. Metheny, and J.C. Schwarzer, 2009, Shear-wave study above Vigindustries, Inc. legacy salt jugs in Hutchinson, Kansas: *Kansas Geological Survey Open-file Report* 2009-3.
- Morton, S.L., J. Ivanov, S. Peterie, R. Miller, B. Bennett, C. Gonzalez, E. Knippel, C. Umbrell, and B. Wedel, 2021, Passive seismic characterization of high priority salt jugs near Hutchinson, Kansas: November 2020: *Kansas Geological Survey Open-file Report* 2021-10, 70 p.
- Morton, S.L., R.D. Miller, J. Ivanov, S.L. Peterie, and, R.L. Parsons, 2020a, Time-lapse monitoring of stress-field variations within the Lower Permian shales in Kansas: *The Leading Edge*, v. 39, no. 5, p. 318-323. doi: 10.1190/tle39050318.1.
- Morton, S.L., S. Peterie, J. Ivanov, R. Miller, B. Bennett, C. Bunker, K. Burke, E. Knippel, J. Lawler, C. Umbrell, and B. Wedel, 2020b, Passive seismic characterization of high priority salt jugs near Hutchinson, Kansas: December 2019: *Kansas Geological Survey Open-file Report* 2020-15, 39 p.
- Park, C., R. Miller, D. Laflen, N. Cabrillo, J. Ivanov, B. Bennett, and R. Huggins, 2004, Imaging dispersion curves of passive surface waves [Exp. Abs.]: Annual Meeting of the Soc. of Expl. Geophys., Denver, Colorado, October 10-15, p. 1357-1360.
- Sayers, C.M., 2004, Monitoring production-induced stress changes using seismic waves [Exp. Abs.]: Annual Meeting of the Soc. of Expl. Geophys., Denver, Colorado, October 10-15, p. 2287-2290.
- Sloan, S.D., R.D. Miller, J. Ivanov, and, S. Walters, 2009, Shear-wave velocity as an indicator of increased stress and failure potential associated with dissolution mining voids: Symposium on the Application of Geophysics to Engineering and Environmental Problems, 363-372. <https://doi.org/10.4133/1.3176713>.
- Sloan, S.D., S.L. Peterie, J. Ivanov, R.D. Miller, and J.R. McKenna, 2010, Void detection using near-surface seismic methods; *in* Advances in Near-Surface Seismology and Ground-Penetrating Radar,

- SEG Geophysical Developments Series No. 15, R.D. Miller, J.D. Bradford, and K. Holliger, eds.: Tulsa, Society of Exploration Geophysicists, p. 201-218.
- Swineford, A., 1955, Petrography of upper Permian rocks in south-central Kansas: State Geological Survey of Kansas Bulletin 111, 179 p.
- Walters, R.F., 1978, Land subsidence in central Kansas related to salt dissolution: Kansas Geological Survey Bulletin 214, 82 p.
- Whittemore, D.O., 1989, Geochemical characterization of saltwater contamination in the Macksville sink and adjacent aquifer: Kansas Geological Survey Open-file Report 89-35.
- Whittemore, D.O., 1990, Geochemical identification of saltwater contamination at the Siefkes subsidence site: Report for the Kansas Corporation Commission.

Appendix

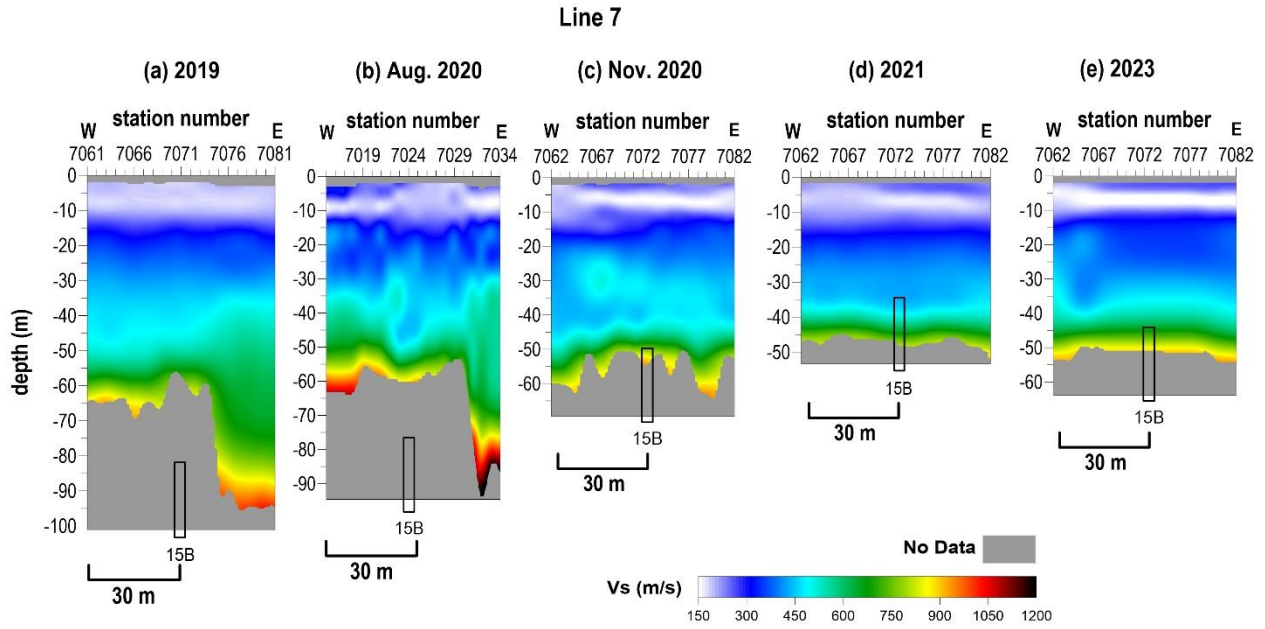


Figure A-1. Shear wave velocity profiles from line 7 in proximity to well 15B for 2015-2020.

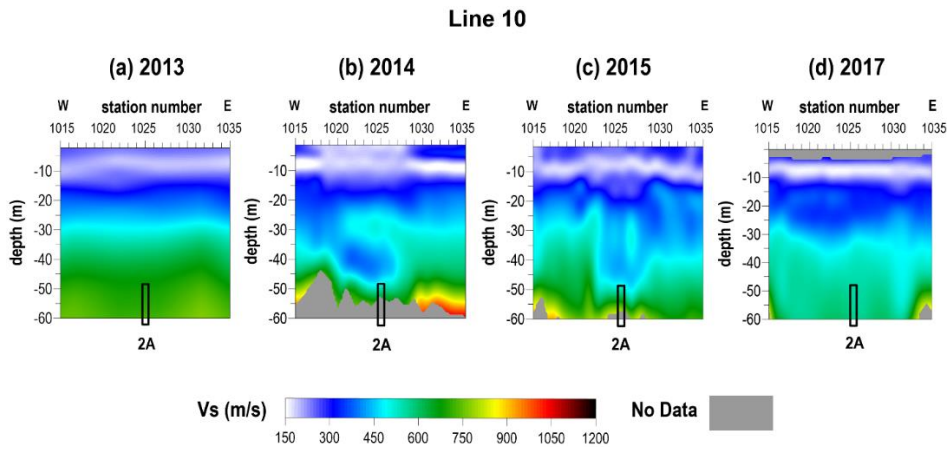


Figure A-2. Shear wave velocity profiles for line 10 over well 2A for 2013-2017.